Journal of Bionic Engineering
https://doi.org/10.1007/s42235-025-00795-5

REVIEW ARTICLE

Bio-inspired Magnetic Helical Miniature Robots: Mechanisms, Control and Biomedical Applications

Aoji Zhu[1] · **Yangmin Li**[1] · **Yongping Zheng**[2] · **Lidong Yang**[1,3]

Received: 23 July 2025 / Revised: 8 September 2025 / Accepted: 11 September 2025

Abstract
Inspired by bacterial motility mechanisms, Magnetic Helical Miniature Robots (MHMRs) exhibit promising applications in biomedical fields due to their efficient locomotion and compatibility with biological tissues. In this review, we systematically survey the basics of MHMRs, from propulsion mechanism, magnetization and control methods to biomedical applications, aiming to provide readers with an easily understandable overview and fundamental knowledge on implementing MHMRs. The MHMRs are actuated by rotating magnetic fields, achieving steering and rotation through magnetic torque, and converting rotation into forward motion through the helical structure. Magnetization methods for MHMRs are reviewed into three types: attaching magnets, magnetic coatings, and magnetic powder doping. Additionally, this review discusses the control methods for MHMRs, covering imaging techniques, path tracking control—including classical control algorithms and increasingly popular learning-based methods, and swarm control. Subsequently, a comprehensive survey is conducted on the biomedical applications of MHMRs in the treatment of vascular diseases, drug delivery, cell delivery, and their integration with catheters. We finally provide a perspective about future challenges in MHMR research, including enhancing functional design capabilities, developing swarm-assisted independent control mechanisms, refining in vivo imaging techniques, and ensuring robust biocompatibility for safe medical use.

Keywords Biologically-inspired robots · Miniature robots · Magnetic control · Biomedical application

1 Introduction

As a cutting-edge branch of robotics, miniature robots possess unique characteristics such as small size (ranging from millimeters to micrometers [1]) and wirelessness, allowing them to enter narrow regions within the human body to perform minimally invasive medical tasks, such as drug delivery [2–4], vascular disease treatment [5–7], hyperthermia therapy [8, 9], etc. Additionally, miniature robots have promising extracorporeal applications, including cell micromanipulation [10, 11], biological detection [12, 13], etc. However, due to their small size, integrating on-board components such as actuators, processors, and power supplies into miniature robots is challenging [1]. At present, researchers have proposed various external field-actuated strategies, including electric fields, optical fields, acoustic fields, magnetic fields, etc [14]. Considering in vivo applications, electric fields pose certain safety risks, optical fields have limited penetration, and acoustic fields exhibit poor steering control [15]. In contrast, magnetic fields are relatively safe for biological tissues, exhibit good tissue penetration and enable real-time steering control. Therefore, magnetic field actuation has gradually become a preferred strategy for externally actuated miniature robots in biomedical applications [16–23].

In microscopic environments, the swimming mechanisms of miniature robots differ significantly from those in macroscopic environments. The Navier–Stokes equation, derived from Newton's second law, describes the behavior of Newtonian fluids as follows:

✉ Lidong Yang
lidong.yang@polyu.edu.hk

[1] Department of Industrial and Systems Engineering, Research Institute for Advanced Manufacturing, The Hong Kong Polytechnic University, Hong Kong 999077, China

[2] Department of Biomedical Engineering, The Hong Kong Polytechnic University, Hong Kong 999077, China

[3] Shenzhen Research Institute, The Hong Kong Polytechnic University, Shenzhen 518057, Guangdong, China

Published online: 16 October 2025

$$-\nabla \boldsymbol{p} + \eta \nabla^2 \boldsymbol{v} = \rho \frac{\partial \boldsymbol{v}}{\partial \mathrm{t}} + \rho(\boldsymbol{v} \cdot \nabla)\boldsymbol{v} \tag{1}$$

where $\boldsymbol{v}$ is the fluid velocity, $\boldsymbol{p}$ is the fluid pressure, ρ is the fluid density and η is the fluid viscosity. The right-hand side of the Navier–Stokes equation (1) represents the inertial forces, while the left-hand side represents the viscous forces. The Reynolds Number (*Re*) is introduced to characterize the ratio of inertial forces to viscous forces: $Re = \frac{\rho v L}{\eta}$, where L represents the characteristic length. Consequently, as the scale of the swimming object decreases, the Reynolds number of its swimming behavior also decreases, leading to a gradual dominance of viscous forces. In low Reynolds number ($Re \ll 1$) environments, the Navier–Stokes equation can be simplified to:

$$\eta \nabla^2 \boldsymbol{v} = \nabla \boldsymbol{p} \tag{2}$$

Since the simplified fluid dynamics equation (2) lacks a time-dependent term, the swimming object exhibits instantaneous and time-reversible characteristics [15]. Consequently, reciprocal motions, such as those of a scallop, cannot generate effective net displacement. This phenomenon is known as the "scallop theorem", proposed by Nobel Prize-winning physicist Purcell in 1977 [24].

To break the scallop theorem, miniature robots require to adopt non-reciprocal motion strategies, such as rotational motion. Nature has inspired numerous bionic robots [25–27]. Back in 1973, biologist Berg et al. demonstrated how *Escherichia coli* swims in liquid through the rotation of its helical flagella [28]. Inspired by bacterial motility mechanisms, researchers have subsequently developed various Magnetic Helical Miniature Robots (MHMRs) [29–31]. These MHMRs effectively convert rotational motion into translational motion under a rotating magnetic field, thereby enabling propulsion in liquid. In 2009, Abbott et al. discussed three effective propulsion mechanisms for magnetic miniature robots in low *Re* environments [32]. Comparison to magnetic field gradient pulling, helical propulsion exhibits superior propulsion efficiency. Compared with traveling wave propulsion, helical propulsion offers comparable propulsion efficiency but has advantages such as simpler reversibility, smoother transition from internal cavities to open environments, and higher manufacturability [32]. Furthermore, MHMRs can achieve efficient three-dimensional propulsion in low-intensity rotating magnetic fields of less than 10 mT, which are safe for human biological systems [33]. By combining the advantages of magnetic field actuation with helical propulsion, MHMRs exhibit substantial potential for in vivo applications.

Over the past two decades, MHMRs have seen significant advancements. In 1996, Honda et al. developed the first MHMR prototype in the world, measuring approximately 21.7 mm in length [29]. In 2005, Kikuchi et al. further downscaled the MHMR to 5.55 mm [34]. In 2007, Bell et al. fabricated the first micron-scale MHMR, termed the artificial bacterial flagellum. This MHMR had a diameter of 3 μm and a length of 30–40 μm, making its size and structure more akin to those of natural microorganisms [30]. Subsequently, in 2009, Ghosh et al. fabricated the first nanoscale MHMR, marking the beginning of the nanotechnology era in this field [35]. In the past ten years, with the development of ultra-precision machining [36–39], imaging technology [40], sensing technology [41, 42] and material technology [43–47], the research trend on MHMRs shows richer functionalities [48–50], improved biocompatibility [51, 52], enhanced environmental adaptability [53, 54], and increased dimensional precision [55, 56] (Fig. 1). Due to the rapid development of technology, a systematic review of the latest MHMR techniques is necessary to engage researchers in related fields and offer tutorial guidance.

Previous reviews on MHMRs inadequately address the fundamental propulsion mechanism and lack a comprehensive discussion on control and magnetization methods [33, 63, 64]. This review systematically surveys the fundamentals of MHMRs, encompassing propulsion mechanisms, magnetization methods, control methods, and biomedical applications. Section 2 commences with the fundamental principles of magnetic torque, gradually analyzing the mechanisms of MHMR steering, rotation, and propulsion, while also introducing current mainstream magnetic field generation systems. Following this, Sect. 3 explores the latest advancements in MHMRs from three magnetization perspectives: attaching magnets, magnetic coatings and magnetic particles doping. These methods function as the "engine" of MHMRs and are closely linked to their fabrication processes. This section will provide guidance on preparing and magnetizing MHMRs according to specific requirements. Building on this foundation, Sect. 4 discusses how to optimize the motion performance of MHMRs through control strategies. It first introduces imaging technologies, including clinically applied methods crucial for ensuring precise control of MHMRs. The section then covers path-following control methods, including traditional and increasingly popular learning-based methods, enabling autonomous navigation in microenvironments. Additionally, it surveys swarm control strategies to enhance tracking efficiency. The preceding sections analyze the latest technologies related to MHMRs, while Sect. 5 focuses on their biomedical applications. Given the unique structure and motion performances of MHMRs, there is extensive research on their roles in vascular clearance, drug transport, cell transport, and their integration with catheters. Finally, Sect. 6 summarizes the review and addresses current research limitations, aiming to

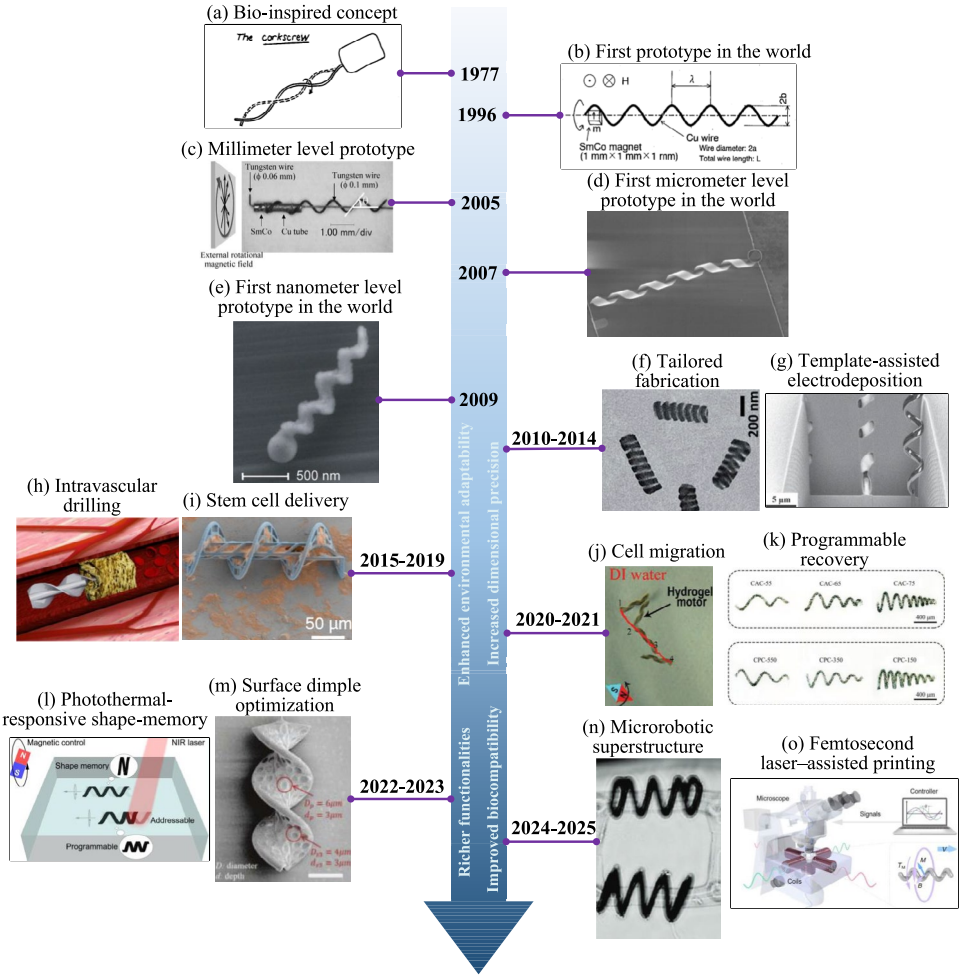

Fig. 1 The historical advancement of MHMRs. **a** Bio-inspired concept [24]. **b** First prototype in the world [29]. **c** Millimeter level prototype [34]. **d** First micrometer level prototype in the world [30]. **e** First nanometer level prototype in the world [35]. **f** Tailored fabrication [57]. **g** Template-assisted electrodeposition [56]. **h** Intravascular drilling [58]. **i** Stem cell delivery [51]. **j** Cell migration [59]. **k** Programmable recovery [60]. **l** Photothermal-responsive shape-memory [52]. **m** Surface dimple optimization [49]. **n** Microrobotic superstructure [61]. **o** Femtosecond laser-assisted printing [62]

inspire further development of MHMRs. The outline of this review is shown in Fig. 2.

2 Propulsion Mechanism

The propulsion mechanism of MHMRs can be summarized in two main processes: Firstly, the rotating magnetic field generates magnetic torque, causing the MHMRs to rotate and steer. This magnetic torque arises from the interaction between the magnetic moment of the MHMR and the externally imposed magnetic field, resulting in synchronous rotation and directional control. Secondly, the intrinsic helical geometry of the MHMRs converts the induced rotational motion into translational propulsion via a corkscrew-like mechanism, analogous to the locomotion observed in certain flagellated microorganisms. In this section, the propulsion mechanism of MHMRs is systematically analyzed from the perspective of fundamental physical principles. Furthermore, various methodologies for the generation of rotating magnetic fields are introduced, encompassing both permanent magnet arrangements and electromagnetic coil systems.

2.1 Magnetic Torque

Within a magnet, the orbital and spin motions of electrons generate magnetic dipoles, which typically neutralize each other due to random atomic arrangements. When an external magnetic field is applied, these dipoles align, resulting in magnetization [68]. The magnitude and direction of the magnetic dipole are described by the magnetic dipole moment $\boldsymbol{m}$, expressed as follows:

$$\boldsymbol{m} = I\boldsymbol{a} \tag{3}$$

where I is the magnitude of the loop current, and $\boldsymbol{a}$ is the area vector of the loop current. The magnetization $\boldsymbol{M}$ of a magnet is defined as the total magnetic dipole moment per unit volume, commonly used to describe its magnetization level.

For paramagnetic materials (e.g., Al, Pd) and diamagnetic materials (e.g., Au, Ag), magnetic dipoles align only

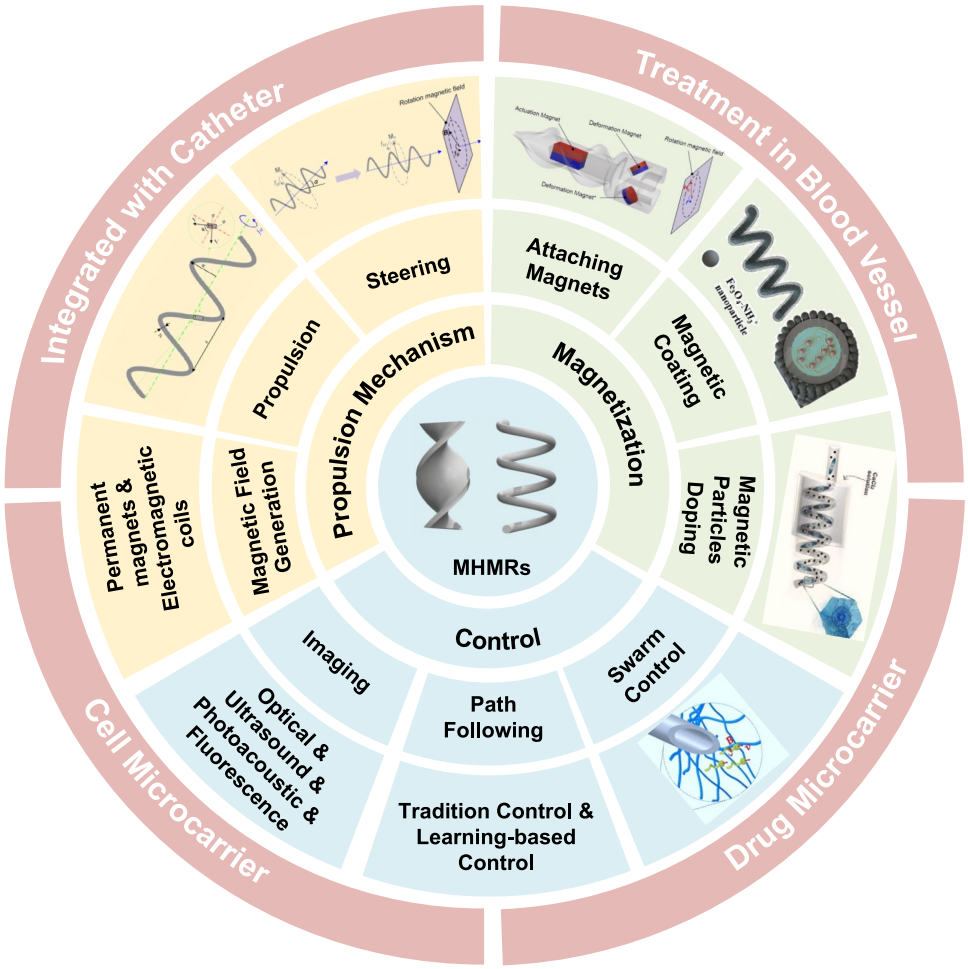

Fig. 2 The outline of this review. Figure source: attaching magnets [48], Magnetic Coating [65], Magnetic Particles Doping [66], Swarm Control [67]

in an external magnetic field. When the field is removed, thermal motion causes the dipoles to revert to a random arrangement, resulting in the loss of magnetism. In contrast, ferromagnetic materials (e.g., Fe, Co, Ni) retain a degree of magnetization even after the external field is removed, known as remanent magnetization $\boldsymbol{M}_r$ [68].

Due to remanent magnetization, permanent magnets made from ferromagnetic materials exhibit magnetism in their natural state. Similar to the magnetization process, when an unfixed permanent magnet is placed in a spatially uniform magnetic field, the field exerts torques on the magnetic dipoles, causing them to align with the external magnetic field (Fig. 3a). The magnetic torque experienced during rotation is expressed as [69]:

$$\boldsymbol{\tau} = V\boldsymbol{M} \times \boldsymbol{B} \tag{4}$$

where V is the magnet volume, $\boldsymbol{M} \approx \boldsymbol{M}_r$, $\boldsymbol{B}$ is the magnetic flux density of the external field, given by $\boldsymbol{B} = \mu_0 (1 + \chi_{\mathrm{m}}) \boldsymbol{H}$, μ_0 is the vacuum permeability, and χ_{m} is the magnetic susceptibility of the hard-magnetic body. The fundamental propulsion principle of MHMRs is intrinsically based on the generation of magnetic torque.

2.2 Steering

MHMRs possess flexible steering capabilities in three-dimensional space. As shown in Fig. 3b, the magnetization direction of MHMRs is oriented radially relative to their helical axis. This specific magnetization configuration enables efficient interaction with externally applied rotating magnetic fields. When the axis of the external rotating magnetic field is not aligned with the axis of the MHMR, a steering magnetic torque is generated. This torque acts to reorient the MHMR, causing it to gradually align its axis with the direction of the external field. The physical mechanism underlying this process is based on the torque experienced by a magnetic dipole in a magnetic field, as described by Eq. (4). The magnitude of the steering magnetic torque can be quantitatively expressed as:

$$\tau_s = V M_r B \sin\alpha \tag{5}$$

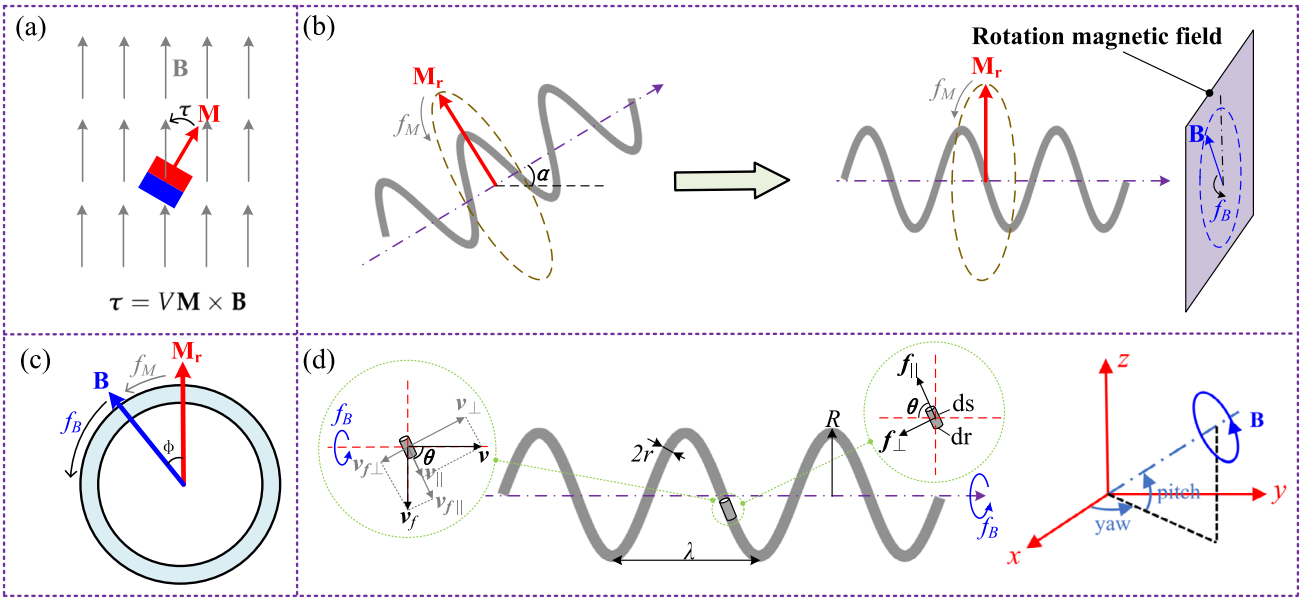

Fig. 3 Schematic diagram illustrating MHMR propulsion in a rotating magnetic field. **a** Magnetic torque exerted on a magnet within a uniform magnetic field. **b** The MHMR steering in a uniform rotating magnetic field B. **c** The MHMR rotates in synchrony with a uniform rotating magnetic field B. **d** A typical MHMR along with its geometric parameters

where α is the angle between the MHMR axis and the rotation axis of external magnetic field. Consequently, by dynamically adjusting the orientation of the rotation axis of the external magnetic field, it is possible to precisely control the rotation direction and trajectory of the MHMR in real time.

2.3 Rotation

The rotation magnetic torque acting on the MHMR is primarily based on torque balance, as described by the following equation:

$$\tau_r = VM_rB\sin\phi = \tau_{drag} = \xi f_M \tag{6}$$

where ξ represents the fluid drag coefficient, typically related to the geometric structure of the MHMR and the physical properties of the surrounding fluid. The f_M is rotation frequency of the MHMR, and ϕ is the angle by which the remanent magnetization of the MHMR lags behind the external magnetic field (Fig. 3c), referred to as the lag angle in this review.

With an increase in the magnetic field frequency, the rotation magnetic torque must also rise to establish a new equilibrium in rotational dynamics, leading to an increase in the lag angle ϕ. Upon lag angle reaching 90°, the rotation magnetic torque (6) achieves its maximal value, causing the MHMR to reach its peak rotation frequency known as the step-out frequency $f_{stepout}$ [70]. If the magnetic field frequency continues to increase, the MHMR will fail to maintain synchronized rotation, as the maximum rotation magnetic torque will no longer be sufficient to overcome the drag torque. Consequently, the correlation between the MHMR rotation frequency f_M and the magnetic field frequency f_B can be expressed as:

$$\begin{aligned} f_M = f_B, f_B \le f_{\text{stepout}} &= \frac{VM_rB}{\xi} \\ f_M \ne f_B, f_B > f_{\text{stepout}} & \end{aligned} \tag{7}$$

Increasing the step-out frequency can expand the operational range of MHMRs. It can be seen from Eq. (7) that increasing the external magnetic field B, enhancing the remanent magnetization M_r, or decreasing the drag coefficient ξ can raise the step-out frequency of MHMR. The external magnetic field can be increased by adjusting the equipment parameters. Enhancing the remanent magnetization can be achieved by using stronger ferromagnetic materials, such as Neodymium-Iron-Boron (NdFeB), which is currently the strongest artificial permanent magnet. Decreasing the drag coefficient can be achieved by adjusting structural parameters or lowering the fluid viscosity.

2.4 Helical Propulsion

Rotational motion is converted into helical propulsion through the helical structure of the MHMR. This mechanism is analogous to the propulsion of bacterial flagella, which rotate to generate thrust in low *Re* environments. Similar to bacterial flagella, the helical structure of the MHMR utilizes

the interplay between external forces and torques to achieve propulsion. At low *Re* environment, there exists a linear relationship between the external forces and torques acting on the helical structure and the resulting propulsion velocity and angular velocity [24]. This correlation is represented by a propulsion matrix [70]:

$$\begin{bmatrix} F \\ \tau \end{bmatrix} = \begin{bmatrix} a & b \\ b & c \end{bmatrix} \begin{bmatrix} v \\ \omega \end{bmatrix} \tag{8}$$

where the propulsion coefficients a, b, and c in the matrix represent the linear factors that depict the inherent connection between the geometric parameters of the helical structure and its propulsion efficacy in fluid environments.

Resistive Force Theory (RFT) is a simplified theoretical framework commonly used to describe the motion of slender structures (e.g., flagella) in viscous fluid environments. It is therefore often applied to study the propulsion mechanisms of MHMRs. RFT simplifies fluid dynamics problems by only considering the local resistive forces acting on the surface of the MHMR. Considering a microelement on a classic MHMR structure (Fig. 3d), the local tangential resistance $f_{\parallel}$ and normal resistance $f_{\perp}$ can be expressed as [71]:

$$\begin{aligned} df_{\parallel} &= Q\xi_{\parallel}\left(v_{\parallel} + v_{\omega\parallel}\right) ds \\ df_{\perp} &= Q\xi_{\perp}\left(v_{\perp} + v_{\omega\perp}\right) ds \end{aligned} \tag{9}$$

where Q denotes the coefficient accounting for interfacial slippage, and ξ represents the local resistance coefficient under the no-slip boundary condition [71]. The tangential resistance coefficient $\xi_{\parallel}$ and the normal resistance coefficient $\xi_{\perp}$ have several formulations, such as those proposed by Gray et al. [72], Cox [73], and Lighthill [74]. For example, the resistance coefficients proposed by Lighthill [74] are expressed as follows:

$$\begin{aligned} \xi_{\perp} &= \frac{4\pi\eta}{\ln\left(\frac{0.36\pi R}{r\sin\theta}\right) + 0.5} \\ \xi_{\parallel} &= \frac{2\pi\eta}{\ln\left(\frac{0.36\pi R}{r\sin\theta}\right)} \end{aligned} \tag{10}$$

where η represents the liquid viscosity, and the other parameters are geometric quantities depicted in Fig. 3d. Integrating over the microelements yields the propulsion coefficients as follows [71]:

$$\begin{aligned} a &= 2n\pi R\left(\frac{\xi_{\parallel}\cos^2(\theta) + \xi_{\perp}\sin^2(\theta)}{\sin(\theta)}\right) Q \\ b &= 2n\pi R^2\left(\xi_{\parallel} - \xi_{\perp}\right)\cos\theta Q \\ c &= 2n\pi R^3\left(\frac{\xi_{\parallel}\sin^2(\theta) + \xi_{\perp}\cos^2(\theta)}{\sin(\theta)}\right) Q \end{aligned} \tag{11}$$

where n denotes the number of helical turns. However, since RFT is a simplified theoretical framework, it has several key limitations. Specifically, RFT cannot account for nonlinear hydrodynamic interactions between the body and the surrounding fluid, nor can it accurately model propulsion in complex geometries or spatially varying environments. These limitations reduce its accuracy in predicting propulsion coefficients under realistic conditions. With the development of finite element simulation techniques, simulation environments now allow for a more accurate investigation of the propulsion coefficients of MHMRs. For example, Hu et al. studied the helical propulsion of MHMRs using numerical simulations, and the experimental results validated that the simulation outcomes were more accurate than those predicted by RFT [75].

With no external magnetic force acting on the MHMR, solely magnetic torque is at play. Hence, based on the propulsion matrix (8), the connection between the rotational frequency and propulsion velocity of the MHMR can be established as follows:

$$v = -\frac{b}{a}\omega = -\frac{2\pi b}{a} f_M \tag{12}$$

where f_M is the rotation frequency of MHMR. Based on the above analysis, the kinematic model of MHMRs in a low Reynolds number free-space 3D environment can be described as follows:

$$\begin{cases} \dot{x} = kf_B\cos(w)\cos(p) \\ \dot{y} = kf_B\sin(w)\cos(p) \\ \dot{z} = kf_B\sin(p) - v_b \end{cases}, \; f_{\text{start}} \le f_B \le f_{\text{stepout}} \tag{13}$$

where $k = -\frac{2\pi b}{a}$, w and p represent the yaw angle and pitch angle of the rotating magnetic field (Fig. 3d), v_b is the drift velocity of the MHMR induced by body forces (e.g., gravitational force and buoyancy), and f_{start} is the start frequency. The start frequency arises because, at low magnetic field frequencies, the forward direction of the MHMR may misalign with its axis due to gravity, buoyancy, or other disturbances, resulting in noticeable oscillations during propulsion. As the rotation frequency of the MHMR increases, the rotation axis gradually aligns with the forward direction, effectively eliminating oscillations and achieving smoother propulsion [63]. Both the start frequency and the step-out frequency can be directly determined through experiments.

2.5 Generation of Magnetic Fields

To achieve effective propulsion and precise control of MHMRs, it is essential to employ a magnetic field generation system that is capable of producing sufficiently strong

and controllable magnetic fields. Magnetic fields suitable for MHMR actuation can be generated using two primary sources: permanent magnets and electromagnetic coils [1].

A magnetic field generation system based on permanent magnets, when integrated with multi-degree-of-freedom robotic arms, can provide a large and highly flexible workspace conducive to various biomedical interventions. Such systems are capable of generating strong and stable magnetic fields while maintaining safety and biocompatibility, thus posing minimal risk to human tissues. Some systems have begun to enter the clinical application stage. The magnetically controlled capsule gastroscope system developed by Ankon Technology (China) has undergone blind trials in Changhai Hospital [76]. Furthermore, in 2023, Stereotaxis (USA) initiated treatments with the newly launched magnetic catheter navigation system, GenesisRMN, on the first group of patients at Advocate Christ Medical Centre. During surgery, doctors use an intuitive computer interface to adjust the magnetic field around the patient. This allows doctors to precisely guide and manipulate a catheter with a permanent magnet embedded in its tip. Despite these advancements, the use of permanent magnets in magnetic field generation systems presents several inherent limitations. The spatial distribution of the magnetic field produced by permanent magnets is highly sensitive to their geometric configuration, material properties, and arrangement. This results in complex magnetic field profiles that often require intricate mathematical modeling, frequently lacking analytical solutions. As a consequence, real-time controllability and fine-tuning of the field are significantly constrained. Furthermore, the inability to instantly switch the magnetic field on or off restricts the immediate initiation or cessation of MHMR movement, which is a critical requirement in many clinical scenarios. The frequency of the generated rotating magnetic field is also determined by the external mechanical actuation of the permanent magnets, thereby imposing upper limits on the achievable field frequency and, consequently, on the propulsion performance and responsiveness of MHMRs.

In contrast, electromagnetic coils offer a vastly superior degree of controllability. By simply adjusting the input current, it is possible to modulate the magnitude, direction, frequency, and temporal dynamics (on/off) of the generated magnetic field with high precision. This dynamic control capability makes electromagnetic coil-based systems the preferred choice among academic researchers, especially for applications necessitating sophisticated trajectory planning and feedback control. The coils commonly used include Helmholtz coils and Maxwell coils [1], but the working space of this coil pair is confined within the coils, making it quite narrow and unsuitable for applications in the human body. Therefore, optimized coil pairs and distributed coils, combined with motion platforms [77, 78], have emerged to enhance the limited working space. The main disadvantages of electromagnetic coils is the safety risks associated with the input current. The generation of strong magnetic fields over large volumes necessitates the use of substantial input currents, often ranging from tens to hundreds of amperes. This high current demand introduces significant thermal effects due to Joule heating, which places stringent requirements on power management, thermal dissipation, and electrical insulation. These factors not only add to system complexity but also pose potential safety hazards to human subjects, particularly in prolonged clinical procedures. Therefore, there is significant room for optimization in the use of electromagnetic coils for magnetic field generation in biomedical applications.

3 Magnetization

The propulsion of the MHMR relies on the magnetic torque generated by its radial magnetization, functioning as its "engine." Thus, integrating a powerful "engine" is fundamental to MHMR research. One simple and cost-effective method is to attach permanent magnets in the helical structure according to the magnetization direction, creating an MHMR. Due to the strong magnetization of permanent magnets, this method provides substantial magnetic propulsion. However, since commercially available magnets typically have a minimum size of around $1\mathrm{mm}$, the overall size of the MHMR is usually limited to the millimeter scale. The position of the magnets can also affect the motion stability of MHMR. This straightforward magnetization approach is often used in navigation control or proof of concept.

Magnetic coating is a post-processing method applied after the helical structure is manufactured and requires radial magnetization. This approach is widely applicable to almost all types of manufactured methods and can achieve sizes as small as 5 μm, making it suitable for many narrow biomedical environments. However, the limitation of this method is that the magnetic coating is thin, resulting in lower magnetization strength and consequently reduced driving force.

Another approach involves doping magnetic particles into the material, allowing the MHMR to be formed directly during the manufacturing process, followed by radial magnetization. This method enables the adjustment of magnetization strength by varying the proportion of magnetic particles, providing sufficient driving force without increasing the volume. Additionally, when combined with biocompatible soft materials, it is well-suited for biomedical applications. However, this method is more complex to prepare, and controlling the dispersion and uniformity of the particles presents challenges, posing a certain entry barrier.

The following discussion will explore the state of the art for MHMRs based on three different magnetization methods: attaching magnets, magnetic coating, and magnetic particles doping. Relevant literature is also presented and summarized in Fig. 4 and Table 1.

3.1 Attaching Magnets

The process of attaching magnets is both straightforward and practical, necessitating only the design and fabrication of a helical structure that incorporates a slot for the magnet. It is recommended to manufacture the helical structure using photopolymer jetting 3D printing, as this allows for secondary curing to secure the magnet within the helical body. As a result, a growing body of conceptual designs and system-level experimental validations have adopted the magnet-attached MHMR approach [48, 79–81]. Kwon et al. addressed the operational efficiency of electromagnetic systems by utilizing magnet-attached MHMRs as actuated objects to minimize the maximum voltage required by magnetic navigation system coils during generation of a rotating magnetic field, thereby optimizing system performance [79] (see Fig. 4a). In another scenario, Zhu et al. introduced a MHMR equipped with two deformation NdFeB magnets and one actuation NdFeB magnet (see Fig. 4b), enabling separate control over object grasping and navigation by adjusting the amplitude and frequency of the magnetic field [48]. Nguyen et al. proposed a guidewire-integrated MHMR designed for excision surgeries in an artificial artery model. The spiral-shaped structure, measuring 9.5 mm in length, was fabricated using photopolymer jetting 3D printing and incorporates a cylindrical NdFeB magnet for magnetic propulsion [81]. Although these design innovations have enabled significant advances in MHMR functionality, challenges remain regarding miniaturization and biocompatibility for real-world biomedical applications. The integration of permanent magnets often results in increased device size and potential cytotoxicity, which must be carefully addressed to ensure safe use in clinical contexts.

MHMRs also offer remarkable flexibility in steering and navigation control, spurring extensive research into automated navigation and magnetic localization strategies. These studies predominantly focus on the development and validation of advanced control and localization algorithms, leveraging the simplicity and cost-effectiveness of magnet-attached MHMRs as experimental platforms [82–87]. Liu et al. investigated the path-tracking capabilities of MHMRs under external disturbances, utilizing an embedded NdFeB

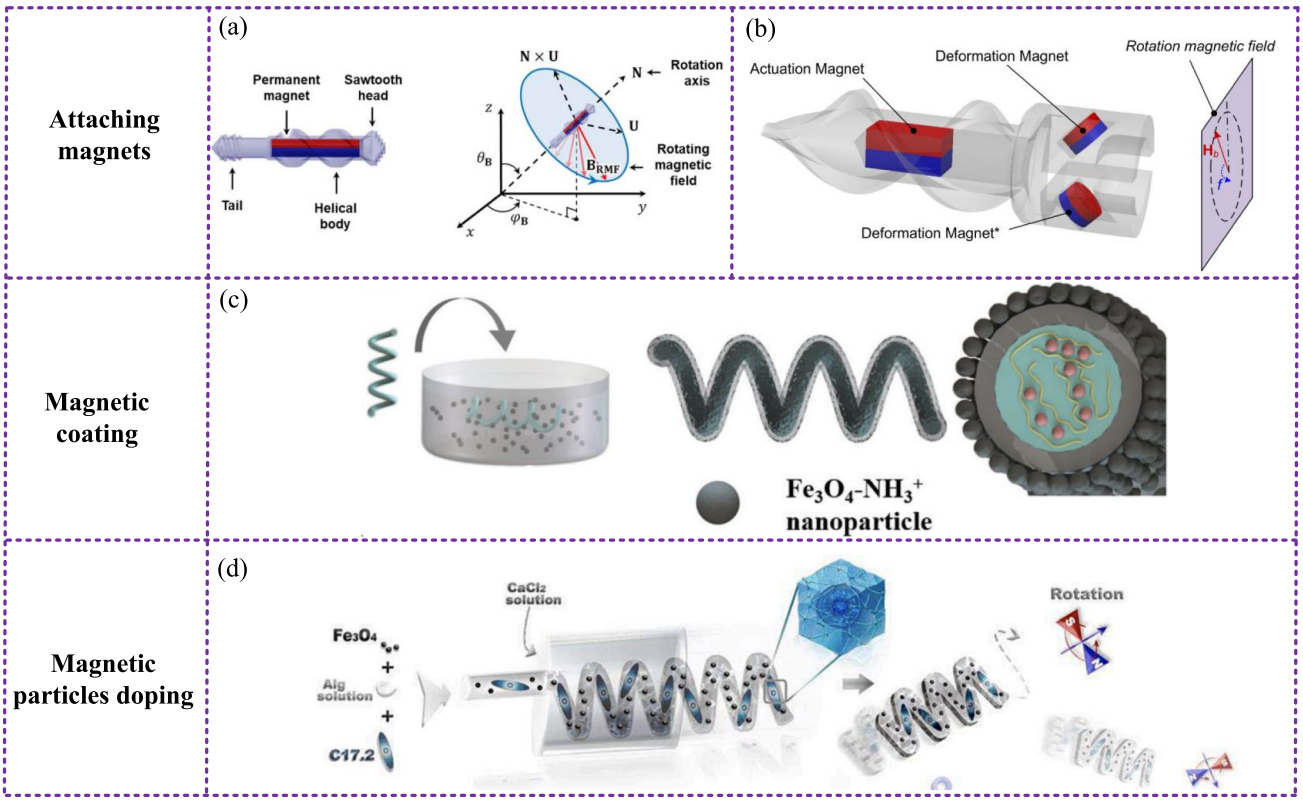

Fig. 4 Schematic diagram illustrating magnetization methods for MHMRs. **a** Embedded magnets are utilized in MHMRs for system validation, used by Kwon et al. [79]. **b** Embedded magnets are utilized in MHMRs for grasping, transporting, and releasing objects, designed by Zhu et al. [48]. **c** Magnetic coating-based MHMR for release control, developed by Liu et al. [65]. **d** Magnetic particles doping-based MHMR for targeted neuronal delivery, developed by Liu et al. [66]

Table 1 Magnetization methods of MHMRs

Magnetization methods	Features	Magnetic material	Main size	Fabrication methods	References
Attaching magnets	Magnetization: *High* Size: *Millimeter-level* Biocompatibility: *Low* Fabrication: *Simple*	NdFeB	10 mm	DLP 3D printing	[48]
		NdFeB	10 mm	DLP 3D printing	[79]
		NdFeB	9.5 mm	PolyJet 3D printing	[81]
		NdFeB	5 mm	Copper spring	[83]
		NdFeB	≈ 8 mm	3D printing	[80]
		NdFeB	10.5 mm	3D printing	[82]
		NdFeB	≈ 10 mm	3D printing	[84]
		NdFeB	14 mm	3D printing	[85]
		NdFeB	2.25 mm	3D printing	[86]
		NdFeB	12 mm	3D printing	[87]
Magnetic coating	Magnetization: *Low* Size: *Micrometer-level* Biocompatibility: *Moderate* Fabrication: *Moderate*	Fe_3O_4	75 μm	TPP 3D printing	[49]
		Ni	20 μm	TPP 3D printing	[88]
		Ni	30 μm	TPP 3D printing	[89]
		Ni	250 μm	TPP 3D printing	[90]
		Ni	≈ 100 μm	TPP 3D printing	[91]
		Ni	≈ 15 μm	TPP 3D printing & sintering	[92]
		Fe_3O_4	26–200 μm	3D helical holographic femtosecond laser	[93]
		Fe_3O_4	≈ 150 μm	*Spirulina platensis*	[40]
		Fe_3O_4	≈ 150 μm	*Spirulina platensis*	[94]
		Fe_3O_4	≈ 150 μm	*Spirulina platensis*	[95]
		Fe_3O_4	560 μm	Microfluidic system	[65]
		Ni	2.5–5 μm	Chemical vapor deposition	[96]
		Ni	200 μm	Plasma-enhanced chemical vapor deposition	[97]
Magnetic particles doping	Magnetization: *Moderate* Size: *Micrometer-level* Biocompatibility: *High* Fabrication: *Hard*	Fe_3O_4	≈ 3 mm	Winding the molten hydrogel	[98]
		NdFeB	1–2 mm	Molding/demolding	[99]
		Fe_3O_4	0.6–1 mm	Microfluidic technology	[66]
		NdFeB	7.5 mm	3D printing	[100]
		Fe_3O_4	100 μm	TPP 3D printing	[101]
		NdFeB	2–3 mm	Winding the NiTi wire	[102]
		NdFeB	6–10 mm	Winding the organo-gel	[103]
		Fe_3O_4	2.5 mm	Winding the PVA	[59]
		Fe_3O_4	20 μm	TPP 3D printing	[104]
		NdFeB	≈ 3 mm	Projection micro-stereolithography 3D printing	[105]
		Fe_3O_4	1–4 mm	Winding the PLA	[52]
		NdFeB	135 μm	TPP 3D printing & VIM	[62]
		Fe_3O_4	2 mm	Bent needle tips integrated system	[106]

permanent magnet for robust magnetic guidance in dynamic environments [82]. Khalil et al. explored magnetic localization by directly attaching an NdFeB magnet to a copper spring, providing insight into the fundamental localization challenges of MHMRs within complex electromagnetic fields [83]. Leclerc et al. advanced the field by performing three-dimensional navigation and conducting blood clot removal experiments in vitro using an MHMR embedded with an NdFeB magnet, thereby demonstrating the translational potential of such systems for minimally invasive interventions [84].

3.2 Magnetic Coating

Magnetic coating is a widely adopted post-processing technique for imparting magnetic functionality to microrobots, typically achieved through sputtering or various physical and chemical deposition methods. Frequently utilized magnetic materials include Nickel (Ni) and Iron Oxide (Fe_3O_4), both of which exhibit favorable magnetic properties and compatibility with a range of substrate materials. The versatility of magnetic coating processes ensures that they can be seamlessly integrated with diverse precision manufacturing methods.

In recent years, Two-Photon Polymerization (TPP) 3D printing has emerged as a cutting-edge technology for ultra-precision additive manufacturing, capable of producing complex three-dimensional micro- and nanostructures with feature sizes down to the sub-100-nanometer scale. The integration of TPP with magnetic coating facilitates the production of MHMRs with dimensions of less than 200 μm [49, 88–93]. Hou et al. designed a dual-helix drill-shaped MHMR measuring 75 μm, which exhibited improved swimming performance through optimized surface dimples, allowing for an adjustable step-out frequency. This MHMR was fabricated using a high-precision TPP system and coated with Fe_3O_4 magnetic nanoparticles suspended in deionized water [49]. Additionally, Yasa et al. investigated the interaction forces between macrophages and the structural parameters of a dual-helix MHMR measuring 20 μm, confirming its immunomodulatory potential for targeted immunotherapy. This MHMR was fabricated using TPP and coated with a nickel layer to impart magnetic properties [88]. Jia et al. designed a hyperbolic cone belt-shaped MHMR measuring 30 μm and conducted simulation analyses of its fluid dynamics and magnetism. Experiments demonstrated its ability to maintain propulsion stability at low frequencies. This MHMR was fabricated using TPP and coated with a nickel layer on its surface [89]. To address the challenge of fabrication throughput, Li et al. introduced a rotary holographic processing strategy that significantly enhances the efficiency of MHMR production. Unlike the conventional point-by-point scanning approach of TPP, this innovative method employs three-dimensionally shaped laser beams to simultaneously process larger volumes, reducing fabrication time to under one second per MHMR. This strategy achieves a fabrication speed approximately 100 times faster than traditional techniques [93].

Spirulina is a naturally occurring helical algae that is edible for both humans and animals, exhibiting excellent biocompatibility. Owing to its intrinsic helical morphology and biodegradable composition, spirulina has attracted considerable interest as a biological template for the fabrication of MHMRs with enhanced biocompatibility. Xie et al., Liu et al. and Li et al. have demonstrated the development of multifunctional MHMRs through the deposition of Fe_3O_4 layers onto spirulina-based microstructures [40, 94, 95]. These coated spirulina MHMRs retain the biological advantages of the template while gaining magnetic responsiveness, enabling wireless actuation, targeted delivery, and multimodal functionalities such as photoacoustic imaging and therapy.

In addition to biological templates, MHMRs can also be fabricated using microfluidic systems, which have gained significant attention in recent years, and combined with magnetic coating for magnetization. Liu et al. employed a microfluidic system to fabricate an MHMR with superior load-bearing capacity, capable of controlled release under environmental stimuli. This MHMR is coated with a polyelectrolyte composite film and Fe_3O_4 nanoparticles, endowing it with robust targeted transport capabilities (Fig. 4c) [65]. To achieve further miniaturization and scalability, chemical vapor deposition techniques have been combined with magnetic coating in the preparation of MHMRs. Bai et al. developed a chemical vapor deposition-based method for the mass production of MHMRs using helical nanowires as structural backbones, which were subsequently coated with a nickel layer to impart magnetic properties. These MHMRs, with dimensions as small as 5 μm, demonstrated effective locomotion under external magnetic fields [96]. Moreover, advancements in chemical vapor deposition have enabled the integration of soft, functional substructures into MHMRs. Hou et al. introduced a plasma-enhanced chemical vapor deposition technique to incorporate nickel-coated soft subcomponents within MHMR architectures. This approach offers a high degree of flexibility in geometric design and enables the extension of propulsion mechanisms by combining rigid and soft elements within a single microrobotic platform [97].

3.3 Magnetic Particles Doping

Magnetic particles doping has emerged as a highly promising strategy for the fabrication of MHMRs, particularly

within the context of biomedical applications. This approach enables the use of inherently biocompatible polymer matrices for constructing complex helical microstructures, while imparting them with the requisite magnetic responsiveness through the homogeneous incorporation of magnetic particles. However, several manufacturing challenges persist. The inclusion of magnetic particles can significantly affect the optical properties such as transparency of photopolymer resins, thereby influencing the efficiency of photopolymerization-based 3D printing. The resulting light scattering and absorption may reduce the curing depth and impact the resolution of the printed microstructures. As a consequence, further research is required to optimize both material formulation and process parameters, ensuring consistent particle dispersion, uniform magnetization, and reliable fabrication outcomes. The two most commonly used classes of magnetic particles in this context are Fe_3O_4 nanoparticles and NdFeB microparticles.

Fe_3O_4 magnetic nanoparticles have become the preferred choice for a wide range of biomedical applications due to their low cost, chemical stability, and superior biocompatibility. Liu et al. reported the development of a hydrogel-based MHMR incorporating Fe_3O_4 nanoparticles, fabricated using a microfluidic chip. This MHMR demonstrated precise transport of neuronal cells to target regions, highlighting its potential in neuronal repair and regenerative medicine (see Fig. 4d) [66]. Similarly, Lee et al. developed a biocompatible and biodegradable MHMR for targeted delivery of anticancer therapeutics. The magnetic actuation was achieved by doping the device with Fe_3O_4 particles, thus combining efficient drug delivery and controlled biodegradation to enhance therapeutic safety and efficacy [101]. Liu further demonstrated the synthesis of MHMRs from Polyvinyl Alcohol (PVA), melamine, water, and Fe_3O_4 nanoparticles, supporting the versatility of this approach across different polymer matrices [98]. In addition to hydrogel systems, various fabrication techniques have been employed to realize Fe_3O_4-doped MHMRs with diverse functionalities. Wang et al. employed a winding technique, mixing Fe_3O_4 particles with PVA and winding the resulting composite onto a rotating needle to fabricate MHMRs for immune cell chemotaxis [59]. Zhao et al. adopted a similar approach, preparing biocompatible MHMRs by mixing Polylactic Acid (PLA) with Fe_3O_4 particles and using a wrapping method for assembly [52]. Moreover, Ceylan et al. integrated Fe_3O_4 nanoparticles into biomacromolecular matrices and utilized dual-photon polymerization 3D printing, resulting in fully degradable MHMRs with precise shape control and reliable magnetic actuation [104]. Inspired by the mechanical principles of chip formation, Fan et al. proposed a simple method for fabricating MHMRs by bending needle tips with Fe_3O_4 particles. Utilizing a multi-degree-of-freedom fabrication platform, needles of various sizes, a compression-thermal fixation strategy, and multiple materials, the substrate, geometry, and size of MHMRs can be adjusted within the range of micrometers to millimeters [106].

While Fe_3O_4 nanoparticles offer excellent biocompatibility, their relatively weak magnetization limits the maximum actuation force achievable. To address this, the use of NdFeB magnetic particles has gained traction, as these particles exhibit much higher remanent magnetization and coercivity. However, the high cost of NdFeB particles and potential concerns regarding their cytotoxicity must be carefully considered, especially for clinical applications. Noteworthy progress has been made in leveraging the superior magnetic properties of NdFeB particles to enhance the performance of MHMRs. Liu et al. designed a multimodal MHMR for navigation and therapeutic assistance in vascular embolization. This device was fabricated by doping a thermoplastic matrix with 20% NdFeB particles and utilizing a thermal stretching process, enabling effective actuation and navigation within blood vessels [99]. Ma et al. and Zhou et al. fabricated MHMRs for vascular clearance using 3D printing of a resin pre-mixed with NdFeB particles, successfully validating the efficacy of the design for removing obstructions in vascular environments and demonstrating the potential of additive manufacturing for complex, magnetically responsive architectures [100, 107]. Moreover, alternative fabrication and material systems have been explored for NdFeB-doped MHMRs. Zhang et al. incorporated NdFeB particles into Polydimethylsiloxane (PDMS) to fabricate the head section of MHMRs, offering both mechanical flexibility and strong magnetic response [102]. Peng et al. utilized a winding method to embed NdFeB particles within a Styrene–Ethylene–Butylene–Styrene (SEBS) elastomeric matrix, yielding MHMRs with robust actuation and thermal stability [103]. Su et al. advanced the field further by employing projection micro-stereolithography 3D printing to fabricate NdFeB particle-doped MHMRs, demonstrating precise magnetic responsiveness and the potential for modularized design and assembly [105]. Wu et al. proposed a femtosecond laser-assisted 3D printing method that combines TPP and Volumetric Injection Molding (VIM), successfully fabricating MHMRs made of hard magnetic material NdFeB [62].

4 Control

The precise motion control of MHMRs relies on the integration of control methods with real-time feedback mechanisms to ensure efficient, accurate, and robust trajectory execution along predefined or dynamically generated paths. Central to the success of MHMR-based interventions is the

ability to continuously monitor and regulate the position, orientation, and velocity of the microrobot within complex environments. For most in vitro applications, optical vision-based feedback effectively provides information regarding the position, orientation, and velocity of the MHMR [108]. In vivo applications, however, require advanced imaging techniques, including ultrasound imaging, photoacoustic imaging, fluorescence imaging, Computed Tomography (CT) imaging and so on. By leveraging feedback on the pose errors of MHMRs, i.e., the deviation between the desired and actual position and orientation control algorithms can be deployed to achieve accurate path following and trajectory correction. Path following control forms the foundation for autonomous navigation in biomedical scenarios, enabling MHMRs to traverse complex and dynamic environments. In addition to single-agent control, the coordinated control of multiple MHMRs, referred to as multi-agent control, has emerged as a promising research frontier. This section will discuss the recent advances in the field of MHMRs from three critical perspectives: imaging and localization techniques, path following control algorithms, and strategies for multi-agent control.

4.1 Imaging

Tracking and pose extraction of MHMRs are fundamental to motion control. Optical imaging, due to its high resolution and real-time capabilities, is the preferred choice for most laboratory studies involving MHMRs, including autonomous navigation algorithm research, proof of concept, and in vitro model experiments. However, for in vivo studies, imaging techniques with tissue penetration capabilities are required.

Ultrasound imaging, which relies on sound wave reflection, is a common clinical imaging technique. It offers advantages such as strong tissue penetration, minimal tissue damage, and good real-time capabilities; however, its spatial resolution is generally moderate, and imaging quality is susceptible to variations in tissue types. Yang et al. developed a system that integrates a mobile electromagnet array and an ultrasound probe, enabling flexible magnetic field generation and ultrasound imaging of MHMRs within a human-scale workspace [7]. Pane et al. combine the 3D kinematic analysis of MHMRs with ultrasound acoustic phase analysis performed on raw radio frequency ultrasound data to enhance imaging and tracking in biological simulation environments [109].

Photoacoustic imaging is a novel imaging method based on the photoacoustic effect, offering greater tissue penetration compared to optical imaging and higher spatial resolution than ultrasound imaging, thereby overcoming the limitations between imaging resolution and depth. However, this imaging method has limited real-time capabilities, and the equipment is relatively expensive and complex to operate. Nonetheless, there are studies related to MHMRs that employ photoacoustic imaging. Xie et al. proposed an MHMR composed of magnetized spirulina and Polydopamine (PDA) on its surface. The introduced PDA coating enhanced photoacoustic and photothermal effects, enabling tracking and photothermal therapy based on photoacoustic imaging [40].

Fluorescence imaging is a widely used medical imaging technique that utilizes the tissue penetration capabilities of fluorescence for in vivo imaging. This technique offers high spatial resolution and sensitivity while enabling real-time imaging. However, fluorescence imaging has limited tissue penetration depth and is susceptible to noise interference from fluorescence scattering, and the need for additional markers increases imaging complexity. Servant et al. labeled the surface of MHMRs with the Near-Infrared (NIR) probe, enabling the first in vivo tracking of a functionalized MHMRs swarm navigating under magnetic control in the peritoneal cavity of mice [110].

4.2 Path Following Control

Path following control for MHMRs can be divided into traditional and learning-based methods. Traditional control encompasses both classical control and model-based modern control theory. These methods have well-established theoretical foundations and are widely applied in industry. While they effectively support the autonomous navigation of MHMRs, they often encounter difficulties when dealing with highly dynamic systems, and their adaptability to complex environments remains limited. In contrast, due to advancements in artificial intelligence for science [111–116], data-driven learning-based methods are gaining traction in the field of robotics. These methods can manage high-dimensional and complex state spaces, making them suitable for intricate tasks in unknown environments and optimizing path tracking strategies. However, learning-based control methods face challenges, including high data requirements and potential stability issues. Relevant literature is also presented and summarized in Fig. 5 and Table 2.

4.2.1 Traditional Methods

As a representative example of classical control theory, Proportional-Integral-Derivative (PID) control was first introduced between the 1920s and 1940s and has since become one of the most widely used and effective control strategies in the field of control systems. With nearly a century of development, PID control has found widespread application in various industrial settings, underscoring its versatility

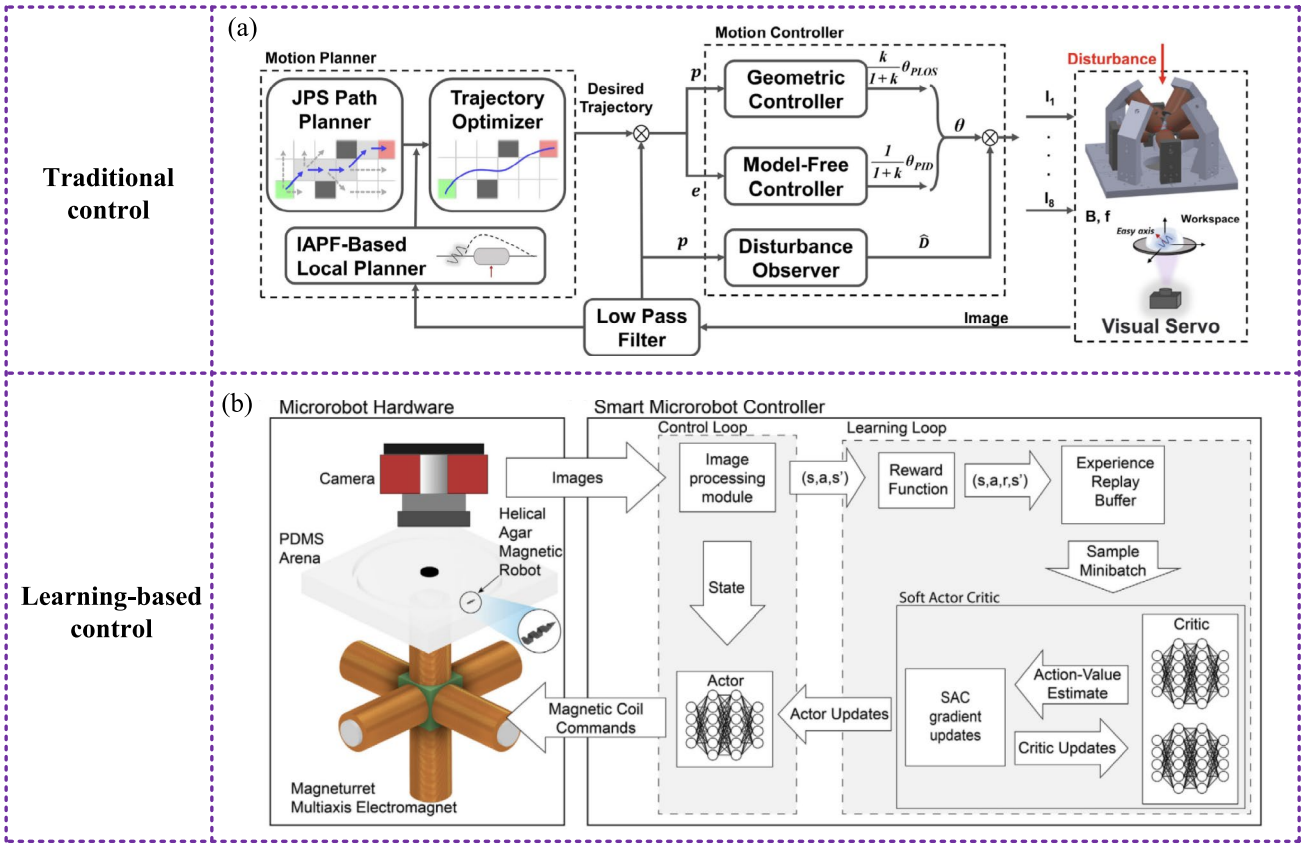

Fig. 5 Schematic diagram illustrating close-loop path following control methods for MHMRs. **a** Path following scheme for MHMRs based on a PID controller and geometric controller, proposed by Zhong et al. [119]. **b** RL strategy for autonomous motion control of hydrogel-based MHMRs, proposed by Behrens et al. [53]

and robustness. One significant advantage of PID controllers is their independence from the precise mathematical model of the controlled system, which simplifies the control mechanism and makes it intuitive for practitioners. These attributes render PID controllers an ideal choice for MHMR control research, where flexibility and ease of implementation are paramount. Fan et al. proposed a control algorithm based on a PI controller integrated with a state extended observer to effectively mitigate magnetic field coupling and external disturbances during the motion tracking of MHMRs [117]. This innovative approach highlights how PID-based strategies can be adapted to address specific challenges in microrobot navigation. Similarly, Zhao et al. developed an automatic control strategy for docking MHMRs, utilizing a PI controller for orientation and steering control [118]. This work illustrates the practical application of PID controllers in enhancing the accuracy of microrobotic operations. Furthermore, Zhong et al. proposed a path-tracking scheme that combines a PID controller with a geometric controller to effectively manage path information. Their research also introduced optimal path planning to achieve autonomous obstacle avoidance and path tracking for MHMRs (Fig. 5a) [119]. Also, the 3D docking path and 3D path-tracking controller designed by Zhao et al., which incorporates a PI controller, enables microrobots to achieve autonomous docking with arbitrarily positioned cylindrical targets in a liquid environment [120].

Compared with classical control, model-based modern control offers stronger theoretical support and higher control accuracy. Excluding the body force-induced drift velocity, the kinematic model of the MHMR (13) is highly stable and depends only on its structural parameters and the external magnetic field, making it quite suitable for model-based modern control approaches. According to different control objectives, model-based modern control can be further categorized into optimal control, robust control, nonlinear control, etc. Optimal control methods mainly include Linear Quadratic Regulator (LQR) and Model Predictive Control (MPC). LQR, based on the assumption of linear systems, obtains the optimal feedback law by optimizing a quadratic performance index. MPC, on the other hand, utilizes receding horizon prediction and optimization, allowing it to handle multiple constraints on inputs and states, albeit at the cost of increased computational complexity. Xu et al. employed an LQR controller to minimize a quadratic cost function, thereby ensuring that the MHMR accurately

Table 2 Path following control methods of MHMRs

Control scheme	Features	Controller	References
Traditional control	Theoretical basis: *Maturity* Adaptability: *Linear, stable* Data Requirement: *Low* Stability: *High*	PI control	[117]
		PI control	[118]
		PID control	[119]
		PI control	[120]
		LQR control	[121]
		MPC	[82]
		Proxy-based SMC	[122]
		Adaptive SMC	[123]
		Nonlinear control	[124]
Learning-based control	Theoretical basis: *Data-driven* Adaptability: *Nonlinear, dynamic* Data Requirement: *High* Stability: *Exist training instability*	LFD-based	[85]
		Imitation learning control	[125]
		RL control	[53]
		RL control	[54]
		DRL control	[126]
		DRL control	[127]
		Data-driven inverse control	[128]
		ELM & FLC	[86]

tracks the reference trajectory while minimizing control effort [121]. Liu et al. designed a planar path-following controller for MHMR based on MPC, achieving better tracking performance compared to the LQR controller [82]. Sliding Mode Control (SMC) represents a robust control approach, achieving strong robustness against external disturbances and model uncertainties through the design of sliding manifolds. Liu et al. introduced a proxy-based framework, where the actual swimmer is virtually coupled with a proxy system. The proxy is controlled using a sliding mode controller, while the actual swimmer follows the proxy, resulting in highly robust path-following control of MHMR in 3D space with adaptive compensation for external disturbances [122]. In addition, Qi et al. proposed an adaptive terminal SMC method combined with a fast terminal disturbance observer to address the issue of input saturation during 3D path following of MHMR [123]. For systems with significant nonlinearity, Lyapunov-based nonlinear control can theoretically guarantee global stability. Xu et al. designed an MHMR path-following controller based on this approach and proved its stability using Lyapunov theory [124].

4.2.2 Learning-based Methods

Despite the significant progress brought by traditional control, these methods mostly rely on accurate mathematical modeling and often struggle to cope with complex, highly dynamic, and uncertain environments. Moreover, the inherent nonlinearity, system parameter variations, and unmodeled disturbances present in real-world applications further limit the effectiveness of traditional controllers. To address these challenges, learning-based control methods have emerged as powerful tools for MHMRs navigation. These methods can be broadly categorized into imitation learning, Reinforcement Learning (RL), data-driven inverse control, and hybrid intelligent control.

Imitation learning collects observation-action pairs from expert demonstrations and employs supervised learning to train control policies, thereby enabling end-to-end control. Xu et al. proposed a data-driven servo control strategy based on Learning from Demonstration (LfD) for MHMR navigation, in which the controller is constructed using the Broad Learning System [85]. Similarly, Li et al. developed an imitation learning-based control method for MHMR navigation [125]. However, imitation learning is highly sensitive to the quantity and diversity of demonstration data, resulting in limited generalization capability. RL, on the other hand, enables the autonomous optimization of control policies by interacting with the environment through trial and error, guided by reward signals. Amoudruz et al. developed a RL-based control strategy for MHMRs, and by comparing it with other algorithms, demonstrated the superiority of RL in achieving minimal-time path planning for MHMRs [54]. Cai et al. designed a soft MHMR and implemented a RL-based flow rate control strategy for navigation and hovering within fluidic pipelines; the controller exhibited robust performance, underscoring the potential of RL in dynamic and complex environments [126]. Furthermore, Behrens constructed a hydrogel-based MHMR and adopted a RL approach for autonomous motion control, highlighting the adaptability and efficiency of RL in various biomedical applications (Fig. 5b) [53]. Wang et al. proposed a deep reinforcement learning (DRL)-based control framework, enabling MHMRs to achieve goal-reaching and dynamic obstacle avoidance [127]. Nevertheless, RL generally requires large amounts of training data, exhibits slow convergence, and faces challenges in stability and sim-to-real transfer. Data-driven inverse control methods learn inverse models of the system online from input–output data, thus enabling adaptive control. Wang et al. proposed a data-driven online inverse controller designed to mitigate environmental and equipment disturbances during autonomous MHMR tracking. This controller allowed MHMRs to successfully complete tracking and obstacle avoidance

tasks with minimal error [128]. However, the accuracy of the model is influenced by the quality of the training data, and its performance varies between linear and nonlinear systems. Hybrid intelligent control combines neural networks with traditional intelligent controllers to achieve higher adaptability and robustness. Liu et al. proposed a radar-based control scheme, where the feedforward controller is based on an Extreme Learning Machine (ELM) neural network and the feedback controller is implemented using a Fuzzy Logic Controller (FLC), enabling automatic navigation of MHMRs in three-dimensional spaces with dynamic obstacles [86]. This approach leverages the powerful modeling capacity of neural networks and the reliability of fuzzy control.

4.3 Swarm Control

The small size and simple structure of magnetic MHMRs present significant challenges in tracking and functionality during various biomedical tasks. To address these limitations, there has been a growing interest in the study of swarm control for MHMRs [67, 71, 129]. The implementation of a swarm approach not only enhances the redundancy and reliability of MHMRs but also increases coverage and improves tracking efficiency, making it particularly advantageous for complex biomedical applications. Moreover, effective swarm control demonstrates a remarkable ability to adapt to environmental changes, further increasing the potential for successful interventions [130, 131]. Wu et al. proposed a swarm of MHMRs specifically designed for drug delivery to the eyes. They utilized clinical optical coherence tomography to track the directional movement of the MHMRs, confirming their successful arrival at the retina. This innovative application highlights the potential of swarm-controlled MHMRs in achieving precise and effective therapeutic outcomes [67].

Current macro-scale robot swarms exhibit strong communication and collaboration capabilities, enhancing their functional efficiency and enabling the execution of more complex tasks. However, this poses significant challenges for MHMRs that lack on-board components. Individual MHMR of swarm requires to exhibit diverse characteristics and possess independent controlled capabilities. Tottori et al. demonstrated the self-propulsion of MHMRs into various configurations under a rotating weak magnetic field, highlighting changes in movement and swimming direction. This study underscores the potential for integrating MHMRs with varying characteristics within a swarm [132]. Additionally, Wang et al. introduced a method for selectively controlling individual MHMRs within a group of geometrically and magnetically identical MHMRs by modifying their surface chemical compositions, showcasing the feasibility of independently selecting specific MHMRs in a swarm [71]. However, current research on the independent control of MHMRs remains superficial, and there is still a considerable gap to achieving effective collaboration within MHMR swarms.

5 Biomedical Applications

Compared to other miniature robots, the characteristics of MHMRs offer unique advantages in biomedical applications. First, the drill-like shape and strong steering capabilities of MHMRs make them promising candidates for minimally invasive treatments in blood vessels. Given that these biomedical tasks require certain rigidity and propulsion capabilities, NdFeB is often considered as the magnetic material, while researchers with appropriate facilities may prefer magnetization methods involving magnetic particles doping. Another popular application direction is using MHMRs as carriers for targeted delivery of drugs or cells. These applications impose higher biocompatibility requirements on MHMRs, leading to a preference for soft materials [133, 134] such as bio-templates and hydrogels as primary materials. Additionally, Fe_3O_4, recognized for its biocompatible magnetic properties, is also favored. Most MHMRs designed for these applications operate at the micrometer scale, making magnetic coating and magnetic particles doping common choices in research efforts. Table 3 and Fig. 6 outlines various research initiatives focusing on the specific biomedical applications of wireless MHMRs, and Fig. 7 shows the biomedical applications of MHMRs integrated with catheter.

5.1 Treatment in Blood Vessel

When abnormal blood clotting occurs due to underlying pathological changes, thrombi may form within blood vessels, potentially leading to severe symptoms in the brain, lungs, or lower limbs, and even posing a life-threatening risk. Rapid, effective, and safe thrombolysis continues to be a significant challenge in biomedical research. The helical structure and propulsion capabilities of MHMRs equip them with the capacity to penetrate and navigate through complex and tortuous vascular environments. Several studies have demonstrated the efficacy of MHMRs in thrombus clearance, each contributing unique insights into their design, functionality, and performance. Hou et al. introduced a concave MHMR capable of efficient propulsion through viscous fluids, successfully penetrating and dispersing thrombi in vitro. The biocompatibility and biodegradability of the MHMR were also verified, highlighting its potential for clinical applications [49]. Building on this, Zhang et

Table 3 Biomedical applications of wireless MHMRs

Specific application	Main materials	Magnetization methods	References
Vascular clearance	GelMA, HAMA, Fe_3O_4	Magnetic coating	[49]
Vascular clearance	PDMS, SMA, NdFeB	Magnetic particles doping	[102]
Vascular navigation	IP-Dip, Ni	Magnetic coating	[51]
Vascular clearance	Unknown resin, NdFeB	Attaching magnets	[80]
Vascular clearance	Loctite epoxy resin, NdFeB	Attaching magnets	[84]
Vascular clearance	Unknown UV Curable Resin, NdFeB	Magnetic particles doping	[100]
Embolization therapy	SEBS, NdFeB	Magnetic particles doping	[99]
Embolization therapy	TAPUA, ACMO, BMA, NdFeB	Magnetic particles doping	[103]
Anticancer drug delivery	PEGDA 700, ethylenediamine, Fe_3O_4	Magnetic particles doping	[101]
Anticancer drug delivery	GelMA, MNPs	Magnetic coating	[3]
Anticancer drug delivery	IP-S, Ni	Magnetic coating	[135]
Photothermal therapy	PLA, Fe_3O_4	Magnetic particles doping	[52]
Photothermal therapy	*Spirulina platensis*, PDA, Fe_3O_4	Magnetic coating	[40]
Photothermal therapy	PVA, melamine, Fe_3O_4	Magnetic particles doping	[98]
Stem cell delivery	IP-Dip, Ni	Magnetic coating	[51]
Stem cell delivery	Alginate hydrogel, Fe_3O_4	Magnetic particles doping	[66]
Inducing stem cell differentiation	*Spirulina platensis*, Fe_3O_4	Magnetic coating	[94]
Inducing stem cell differentiation	Gelma, MENPs	Magnetic coating	[136]
Directing cell chemotaxis	PVA, melamine, Fe_3O_4	Magnetic particles doping	[59]
Cell delivery	plasma, albumin, platelet lysate, Fe_3O_4	Magnetic particles doping	[104]
Cell delivery	AAc, MAAc, NIPAAM, PVP, NdFeB	Magnetic particles doping	[105]
Assisted reproduction	IP-DIP, Fe	Magnetic coating	[137]

al. proposed a shape-transforming MHMR that enhanced thrombus clearance efficiency by adapting its form to better engage with and disrupt thrombus structures. This adaptability, paired with biocompatibility, underscores its promise as an effective thrombolytic tool [102]. Further advancing the field, Jeon et al. conducted vascular navigation experiments in mouse brains, demonstrating the ability of MHMRs to navigate through intricate vascular networks (Fig. 6a) [51]. These findings are complemented by additional studies that reinforce the exceptional navigation and thrombus clearance capabilities of MHMRs within vascular environments. For instance, Ma et al., Yang et al., and Leclerc et al. validated the potential of MHMRs to traverse blood vessels and efficiently remove thrombi, further establishing their therapeutic promise [80, 84, 100].

In addition to thrombus clearance, MHMRs are emerging as a promising tool in embolization therapy, which involves blocking specific blood vessels to control bleeding or treat pathological conditions. Their superior navigational capabilities make them well-suited for precise interventions in vascular environments. Liu et al. introduced a soft-material MHMR capable of switching between navigation and embolization modes using external magnetic fields. This dual functionality was validated in a rabbit femoral artery model, demonstrating the effectiveness of MHMRs in embolization therapy [99]. Similarly, Peng et al. showcased the potential of MHMRs for rapid vascular occlusion, successfully performing an MHMR-based embolization procedure in the rabbit renal artery. The swift and effective occlusion of the target vessel underscores the ability of MHMRs to execute complex therapeutic tasks with high efficiency and precision (Fig. 6b) [103].

5.2 Drug Microcarrier

MHMRs represent a highly promising advancement in the precise delivery of therapeutic agents to diseased regions, significantly broadening their applications in biomedicine. In particular, MHMRs have demonstrated substantial potential to improve the efficacy of cancer treatment and bacterial infection therapy compared to traditional methods such as injection and oral administration. A key focus of MHMR-based research has been their application in targeted drug delivery, especially in cancer therapy. Lee et al. developed a biocompatible and biodegradable MHMR capable of delivering the chemotherapeutic agent doxorubicin to tumor sites. The release of the drug was triggered by NIR light stimulation, demonstrating precise control over drug delivery [101]. Building on this design, they advanced the technology to create an MHMR that sequentially delivered two distinct drugs?gemcitabine and doxorubicin. The dual–drug delivery system utilized NIR light and self-decomposition mechanisms to activate drug release, significantly enhancing therapeutic efficacy against cancer cells (Fig. 6c) [3]. In addition to these developments, Lee et al. also designed a needle-shaped MHMR capable of carrying the chemotherapeutic agent paclitaxel. This design demonstrated its practicality in targeting microtissues within physiological environments, further highlighting the versatility and precision of MHMRs in drug delivery applications [135].

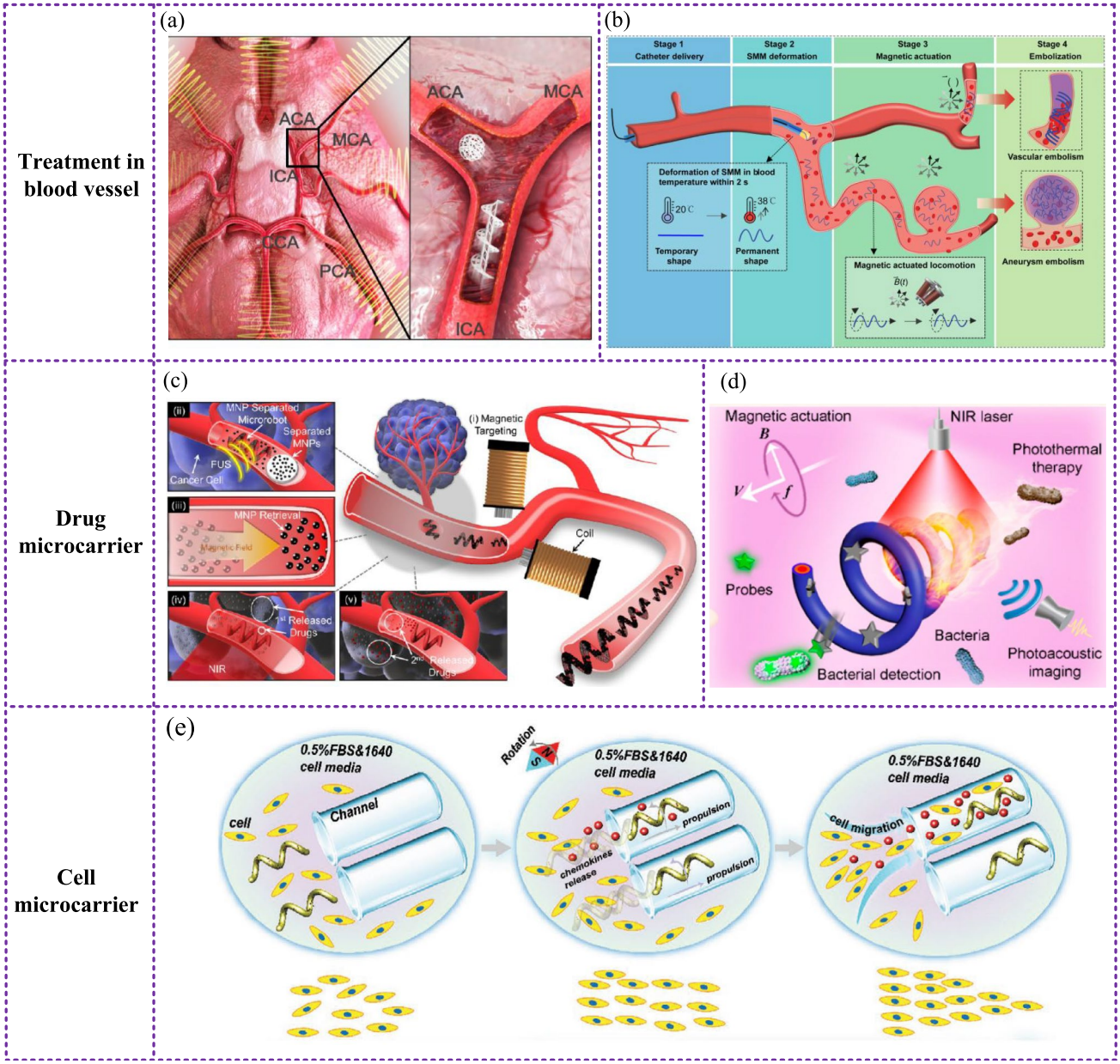

Fig. 6 Schematic diagram illustrating the biomedical applications for wireless MHMRs. **a** Biocompatible MHMR for vascular clearance, developed by Jeon et al. [51]. **b** Biocompatible MHMR for embolization therapy, developed by Peng et al. [103]. **c** Biocompatible and Biodegradable MHMR for anticancer drug delivery, developed by Lee et al. [3]. **d** Biocompatible MHMR for PTT, developed by Xie et al. [40]. **e** Biocompatible and Biodegradable MHMR for directing cell chemotaxis, developed by Wang et al. [59]

Beyond direct drug delivery, MHMRs have also been explored for Photothermal Therapy (PTT), a strategy that uses photothermal agents to convert NIR light into localized heat. This heat induces a temperature increase in the target area, promoting apoptosis of diseased cells or bacteria while minimizing damage to surrounding healthy tissues. Zhao et al. introduced an MHMR capable of morphological transformation in response to temperature changes, demonstrating its effectiveness in PTT applications for cancer therapy [52]. Similarly, Xie et al. developed an MHMR based on spirulina coated with Polydopamine (PDA). This system effectively activated a photothermal effect under NIR laser irradiation, showcasing its efficacy in treating bacterial infections, particularly Klebsiella infections (Fig. 6d) [40]. Further advancing the field, Liu et al. fabricated an MHMR using hydrogel as the base material. This design enabled the targeted delivery of photothermal agents, achieving a localized eradication rate exceeding 60% for HeLa cells [98]. These findings highlight the versatility of MHMRs

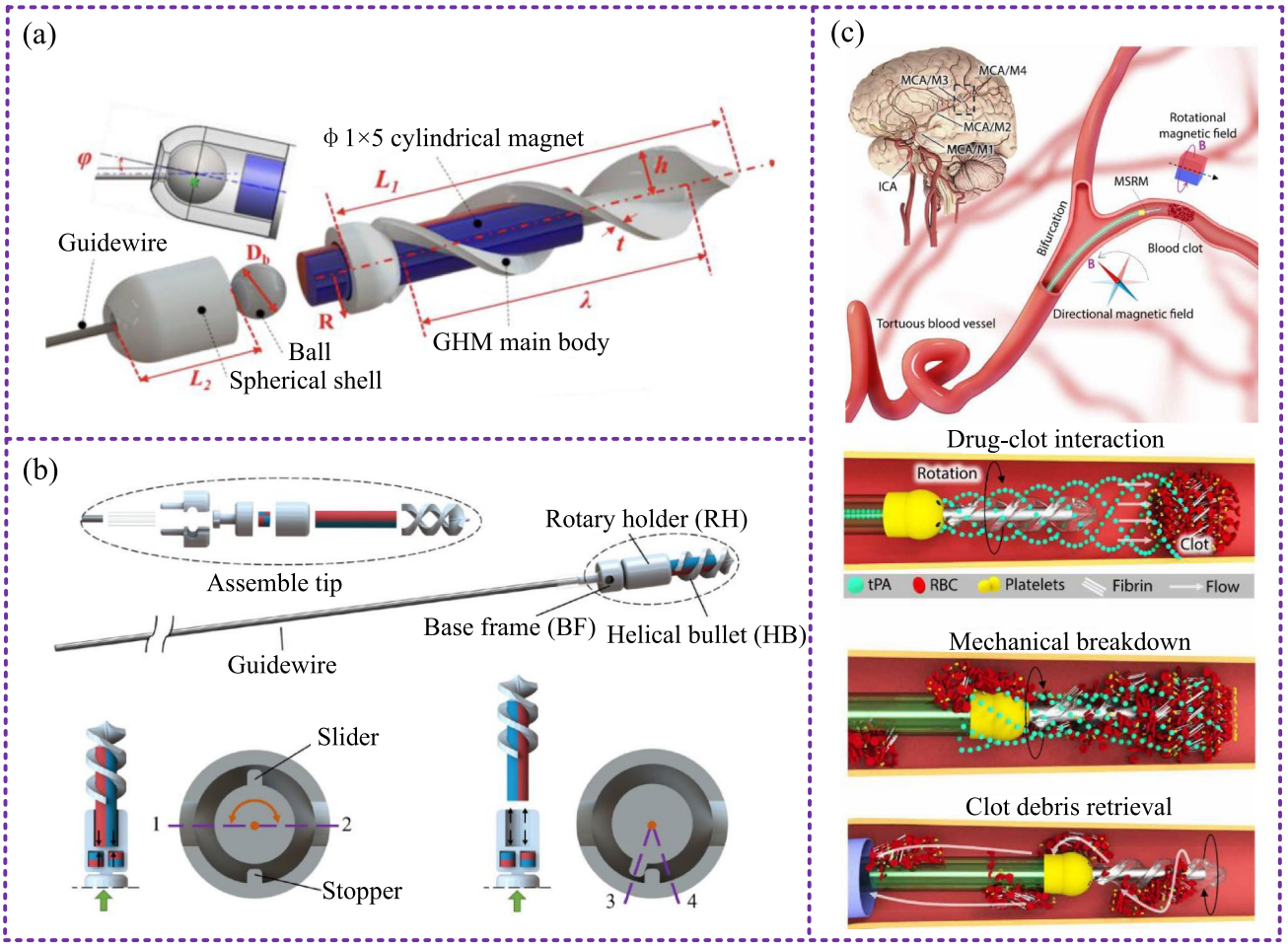

Fig. 7 Schematic diagram illustrating the integration of MHMRs with catheters for biomedical applications. **a** A MHMR integrated with guidewire for mechanical atherectomy in narrow blood vessels, developed by Nguyen et al. [81]. **b** A novel design enabled the seamless release and retrieval of the MHMR from catheter, developed by Yang et al. [138]. **c** Biocompatible soft MHMR integrated with guidewire for thrombus treatment, developed by Zhang et al. [139]

in combining drug delivery with photothermal effects to enhance therapeutic outcomes.

5.3 Cell Microcarrier

In addition to drug delivery, MHMRs have shown potential as carriers for cell-based applications in biomedicine. One promising application of MHMRs is in neuronal repair, where they facilitate the cultivation, transportation, and implantation of stem cells to target regions. Jeon et al. successfully utilized MHMRs to cultivate and proliferate hippocampal neural stem cells, demonstrating their ability to precisely deliver these cells to target areas [51]. Building on this, Liu et al. employed MHMRs to promote the regeneration of neurons in African clawed frogs, further highlighting their potential in neurological applications [66]. More innovative designs have incorporated piezoelectric materials into MHMRs to enhance their functionality. For example, Liu et al. developed spirulina-based MHMRs coated with piezoelectric materials that, when stimulated by ultrasound, generated electrical signals to induce stem cell differentiation [94]. Similarly, Dong et al. demonstrated the use of MHMRs for stem cell transportation and differentiation, where electrical signals played a critical role in guiding stem cell behavior [136].

MHMRs have also been explored for their ability to guide immune cells, offering new possibilities for immunotherapy. Wang et al. designed hydrogel-based MHMRs capable of delivering chemotactic factors to immune T cells. This approach successfully directed T cell migration and modulated immune responses, showcasing the potential of MHMRs to enhance immune cell targeting and therapeutic outcomes (Fig. 6e) [59]. To address biocompatibility and safety concerns, researchers have explored constructing MHMRs from human-derived biomaterials. For example, Ceylan et al. utilized patient-derived blood-based biomaterials to construct MHMRs that undergo hydrolysis under protease activity, reducing cytotoxicity and ensuring safer

applications [104]. Similarly, Su et al. employed cell scaffolds to create MHMRs capable of effective cell loading and transportation. These MHMRs demonstrated safe on-demand cell release in rabbit bile ducts, further validating the feasibility of such designs in clinical scenarios [105].

In the field of assisted reproduction, MHMRs have shown potential as microcarriers for sperm cells, enabling targeted delivery to oocytes to enhance fertilization. Xu et al. proposed an integrated MHMR system designed for the directed transport of sperm within the reproductive system. This system combines MHMRs with hyaluronic acid microlayers, which allow for in situ selection and transport of multiple sperm cells. Once transported, the microlayers are hydrolyzed by localized proteases, releasing the sperm to reach their target location [137].

5.4 Integrated with Catheter

Wireless MHMRs have demonstrated great potential in minimally invasive interventions and perform therapeutic tasks. However, several limitations hinder their practical application in vivo. These include difficulties in retrieval, the risk of losing the device within the body, and potential health hazards caused by unintentional retention. To address these challenges, researchers have explored integrating MHMRs with catheters in recent years, offering better control, safety, and retrievability during clinical procedures. Nguyen et al. integrated a MHMR at the tip of a thin guidewire for mechanical atherectomy in narrow blood vessels. The developed prototype utilized an advanced electromagnetic navigation system to efficiently perform steering and drilling motions in angiographic environments while maintaining the tip at the vessel center to avoid perforation (Fig. 7a) [81]. Similarly, Yang et al. incorporated a MHMR at the distal tip of the guidewire, monitored via radiation-free ultrasound imaging, achieving a preliminary verification of catheter operations combining magnetic navigation and unclogging motions under ultrasound guidance [7]. Building on this foundation, Yang et al. further improved the integration of the MHMR with the guidewire by designing a slider mechanism. This novel design enabled the seamless release and retrieval of the MHMR, significantly enhancing operational safety and practicality (Fig. 7b) [138]. Advancing the concept further, Dreyfus et al. proposed a highly flexible continuum guidewire robot integrated with MHMR. The inclusion of an articulating magnetic tip allowed for active and controllable steering, enabling precise navigation from the aortic arch to millimeter-sized arteries in the brain [5]. Furthermore, Zhang et al. introduced a guidewire integrated with a soft MHMR, specifically designed to access small blood vessels and provide efficient, minimally invasive therapeutic interventions for thrombus treatment. This innovative design was successfully validated in in vivo rabbit models, demonstrating its potential for clinical applications (Fig. 7c) [139].

6 Conclusion and Future Prospects

This review provides a comprehensive survey of the propulsion mechanism, magnetization, and control methods of MHMRs, highlighting the latest advancements in their biomedical applications. The magnetic torque induced by a rotating magnetic field enables MHMRs to achieve flexible steering while allowing them to rotate around their central axis, utilizing the helical structure for forward propulsion at related speeds proportional to their rotational frequency, up to a step-out frequency. Recent advancements classify MHMR magnetization into three distinct modes: attaching magnets, magnetic coating, and magnetic particles doping. Attaching magnets directly onto MHMRs offers a simple, cost-effective method for strong magnetic propulsion, usually limited to the millimeter scale. Magnetic coating allows application across small to micrometer scales in diverse materials and manufacturing methods. Doping magnetic particles into MHMR materials enables micrometer-scale use with effective magnetic propulsion, requiring expertise in material preparation. Imaging of MHMRs is fundamental for motion control. In addition to optical imaging, various in vivo imaging techniques, including ultrasound imaging, photoacoustic imaging, and fluorescence imaging, have been developed for tracking MHMRs. Control methods for MHMRs have developed into two primary categories: traditional methods, including PID, LQR, MPC and SMC, and learning-based methods, such as imitation learning and reinforcement learning. Furthermore, research on swarm control of MHMRs has contributed to improved tracking efficiency. In biomedical applications, MHMRs demonstrate promises in the treatment of vascular diseases, including vascular clearance and embolization therapy. MHMRs can also serve as drug microcarriers for targeted delivery of anticancer drugs or for delivering photothermal agents for PTT. Additionally, MHMRs as cellular microcarriers show their utility in applications such as stem cell transplantation, immune cell chemotaxis and assisted reproduction. In addition to wireless MHMRs, their integration with catheters has also been discussed.

MHMRs have rapidly developed but several challenges still remain for researchers to address, which can be summarized in four key areas:

Tailored functional design for helical propulsion Unlike other microscale robots, MHMRs rely on helical structures to convert rotating magnetic fields into propulsive forces through corkscrew-like motion. Current MHMRs often

use single-material, rigid helices, which limits their performance in complex biological environments. Future research should prioritize the development of hybrid and soft helical architectures capable of dynamically adjusting their shape and stiffness in response to varying tissue environments or propulsion demands. For instance, tunable helical pitch or flexible tail designs could enhance propulsion efficiency and facilitate navigation through heterogeneous media, including mucus, blood, or extracellular matrix, which present unique challenges for helical propulsion. Furthermore, incorporating additional functionalities, such as magnetically controlled shape morphing [103, 140], onboard drug reservoirs, or localized heating for hyperthermia, directly into the helical body could expand the biomedical applications of MHMRs. The multimodal designs presented in [140–143] and the advanced control strategies for multi-robot interactions in confined spaces discussed in [144] are more generalized studies on magnetic miniature robots. These works provide valuable background and inspiration for enhancing the multimodal functional capabilities of MHMRs. By drawing on these broader design principles and control strategies, future MHMR development can further improve their adaptability and performance in complex in vivo environments.

Swarm and cooperative control leveraging helical dynamics Swarm control in MHMRs presents challenges distinct from other microrobot types due to the coupling between magnetic field actuation and helical propulsion. Unlike photonic or chemical swarms, where local actuation is possible, all MHMRs in the same field experience similar torques, making independent control nontrivial. Future research should explore the exploitation of subtle differences in helical geometry (e.g., pitch, diameter, magnetic susceptibility), resonance phenomena, or multi-frequency magnetic field strategies to selectively address individuals within a swarm. Additionally, the dynamics of hydrodynamic coupling between MHMRs are still not fully understood and may be leveraged to achieve emergent, collective behaviors unique to MHMRs. The development of real-time feedback control systems using magnetic field shaping, together with AI-driven controllers that adapt to both field-microstructure interactions and biological flows, will be key to enabling complex cooperative tasks such as cargo transport, collective sensing, or targeted therapy.

In vivo imaging and real-time magnetic localization Precise in vivo imaging and localization of MHMRs is especially challenging due to their small magnetic signatures and the complexity of biological fluids. Unlike optically driven robots, MHMRs require imaging modalities that can detect their 3D position and orientation under magnetic actuation, often in deep tissues where optical access is limited. Future directions should focus on the integration of magnetic particles imaging, advanced magnetic resonance imaging sequences tailored for helical propulsion, or real-time electromagnetic tracking systems that can resolve both the translational and rotational dynamics of MHMRs. The development of magnetic contrast agents specifically designed for helical geometry may further improve the detectability and safety of these robots in vivo. Importantly, integrating imaging with closed-loop magnetic control will be crucial for achieving safe, precise interventions in clinical settings.

Biocompatibility and long-term fate of magnetically driven helical structures The unique requirements for strong and responsive magnetic materials in MHMRs present biocompatibility challenges distinct from other propulsion modalities. The incorporation of magnetic nanoparticles or permanent magnets within helical bodies raises concerns regarding cytotoxicity, immunogenicity, and long-term tissue integration. Unlike chemically or acoustically driven robots, MHMRs must balance the need for robust magnetic actuation with the demands of safe degradation or clearance from the body. Future research should prioritize the development of biodegradable magnetic composites, surface coatings that minimize immune responses, and systematic studies on the fate of helical microstructures after task completion. Additionally, there is a need for standardized in vivo evaluation protocols specifically tailored to the unique motion and material properties of MHMRs to ensure their safety and efficacy in translational medicine.

Acknowledgements The authors would like to express their sincere thanks to the financial support from the Research Institute for Advanced Manufacturing (RIAM) of The Hong Kong Polytechnic University (project Nos. 1-CD9F and 1-CDK3), the Research Grants Council (RGC) of Hong Kong (project Nos. 25200424 and 15206223), the GuangDong Basic and Applied Basic Research Foundation (project No. 2023A1515110709), and the Startup fund (project No. 1-BE9L) of the Hong Kong Polytechnic University. Aoji Zhu is also supported by grant from the Research Committee of the Hong Kong Polytechnic University under student account code RN5Y.

Author Contributions Aoji Zhu: Writing the initial draft; Review and editing; Yangmin Li: Review and editing; Yongping Zheng: Review and editing; Lidong Yang: Review and editing; Supervision; All authors have read and agreed to the published version.

Funding Open access funding provided by The Hong Kong Polytechnic University

Data Availability All data generated or analysed during this study are included in this published article.

Declarations

Conflict of interest The authors have no relevant financial or nonfinancial interests to disclose.

References

1. Yang, Z., & Zhang, L. (2020). Magnetic actuation systems for miniature robots: A review. *Advanced Intelligent Systems, 2*(9), 2000082. https://doi.org/10.1002/aisy.202000082
2. Nelson, B. J., & Pané, S. (2023). Delivering drugs with microrobots. *Science, 382*(6675), 1120–1122. https://doi.org/10.1126/science.adh3073
3. Lee, H., & Park, S. (2023). Magnetically actuated helical microrobot with magnetic nanoparticle retrieval and sequential dual–drug release abilities. *ACS Applied Materials & Interfaces, 15*(23), 27471–27485. https://doi.org/10.1021/acsami.3c01087
4. Li, M., Wu, J., Li, N., Zhou, J., Cheng, W., Wu, A., Liu, L., & Jiao, N. (2024). Cross-scale drug delivery of diatom microrobots based on a magnetic continuum robot for combined chemical and photodynamic therapy of glioblastoma. *Advanced Functional Materials, 34*(37), 2402333. https://doi.org/10.1002/adfm.202402333
5. Dreyfus, R., Boehler, Q., Lyttle, S., Gruber, P., Lussi, J., Chautems, C., Gervasoni, S., Berberat, J., Seibold, D., Ochsenbein-Kölble, N., Reinehr, M., Weisskopf, M., Remonda, L., & Nelson, B. J. (2024). Dexterous helical magnetic robot for improved endovascular access. *Science Robotics, 9*(87), 0298. https://doi.org/10.1126/scirobotics.adh0298
6. Li, T., Yu, S., Sun, B., Li, Y., Wang, X., Pan, Y., Song, C., Ren, Y., Zhang, Z., Grattan, K. T. V., Wu, Z., & Zhao, J. (2023). Bio-inspired claw-engaged and biolubricated swimming microrobots creating active retention in blood vessels. *Science Advances, 9*(18), 4501. https://doi.org/10.1126/sciadv.adg4501
7. Yang, Z., Yang, L., Zhang, M., Zhang, C., Yu, S. C. H., & Zhang, L. (2021). Ultrasound-guided catheterization using a driller-tipped guidewire with combined magnetic navigation and drilling motion. *IEEE/ASME Transactions on Mechatronics, 27*(5), 2829–2840. https://doi.org/10.1109/TMECH.2021.3121267
8. Sridhar, V., Yildiz, E., Rodríguez-Camargo, A., Lyu, X., Yao, L., Wrede, P., Aghakhani, A., Akolpoglu, B. M., Podjaski, F. M., Lotsch, B. V., & Sitti, M. (2023). Designing covalent organic framework-based light-driven microswimmers towards intraocular theranostic applications. *Investigative Ophthalmology & Visual Science, 64*(8), 5025–5025. https://doi.org/10.1002/adma.202301126
9. Xing, G., Yu, X., Zhang, Y., Sheng, S., Jin, L., Zhu, D., Mei, L., Dong, X., & Lv, F. (2024). Macrophages-based biohybrid microrobots for breast cancer photothermal immunotherapy by inducing pyroptosis. *Small, 20*(7), 2305526. https://doi.org/10.1002/smll.202305526
10. Wang, F., Zhang, Y., Jin, D., Jiang, Z., Liu, Y., Knoll, A., Jiang, H., Ying, Y., & Zhou, M. (2024). Magnetic soft microrobot design for cell grasping and transportation. *Cyborg and Bionic Systems, 5*, 0109. https://doi.org/10.34133/cbsystems.0109
11. Iványi, G. T., Nemes, B., Gróf, I., Fekete, T., Kubacková, J., Tomori, Z., Bánó, G., Vizsnyiczai, G., & Kelemen, L. (2024). Optically actuated soft microrobot family for single-cell manipulation. *Advanced Materials, 36*(32), 2401115. https://doi.org/10.1002/adma.202401115
12. Chen, H., Zhou, T., Li, S., Feng, J., Li, W., Li, L., Zhou, X., Wang, M., Li, F., Zhao, X., & Ren, L. (2023). Living magnetotactic microrobots based on bacteria with a surface-displayed crispr/cas12a system for penaeus viruses detection. *ACS Applied Materials & Interfaces, 15*(41), 47930–47938. https://doi.org/10.1021/acsami.3c09690
13. Zhang, Y., Zhang, L., Yang, L., Vong, C. I., Chan, K. F., Wu, W. K., Kwong, T. N., Lo, N. W., Ip, M., Wong, S. H., Sung, J. J. Y., Chiu, P. W. Y., & Zhang, L. (2019). Real-time tracking of fluorescent magnetic spore-based microrobots for remote detection of c. diff toxins. *Science Advances, 5*(1), 9650. https://doi.org/10.1126/sciadv.aau9650
14. Wang, Q., & Zhang, L. (2021). External power-driven microrobotic swarm: From fundamental understanding to imaging-guided delivery. *ACS Nano, 15*(1), 149–174. https://doi.org/10.1021/acsnano.0c07753
15. Zhou, H., Mayorga-Martinez, C. C., Pané, S., Zhang, L., & Pumera, M. (2021). Magnetically driven micro and nanorobots. *Chemical Reviews, 121*(8), 4999–5041. https://doi.org/10.1021/acs.chemrev.0c01234
16. Chen, Z., Wang, Y., Chen, H., Law, J., Pu, H., Xie, S., Duan, F., Sun, Y., Liu, N., & Yu, J. (2024). A magnetic multi-layer soft robot for on-demand targeted adhesion. *Nature Communications, 15*(1), 644. https://doi.org/10.1038/s41467-024-44995-9
17. Fischer, F., Gletter, C., Jeong, M., & Qiu, T. (2024). Magneto-oscillatory localization for small-scale robots. *NPJ Robotics, 2*(1), 1. https://doi.org/10.1038/s44182-024-00008-x
18. Yang, W., Liu, H., Guo, Q., Wang, W., Yu, H., & Liu, A. (2024). Expansion of self-assembled structures of heteroarray ndfeb semicircular arc magnetic minirobots. *Journal of Bionic Engineering, 21*(5), 2258–2270. https://doi.org/10.1007/s42235-024-00544-0
19. Iacovacci, V., Diller, E., Ahmed, D., & Menciassi, A. (2024). Medical microrobots. *Annual Review of Biomedical Engineering, 26*, 561–591. https://doi.org/10.1146/annurev-bioeng-081523-033131
20. Zhang, H., Luo, K., Wang, F., Li, S., Meng, X., & Xie, H. (2025). Development of a magnetically-actuated capsule robot for biopsy sampling using sma. *Journal of Bionic Engineering, 22*, 1609–1621. https://doi.org/10.1007/s42235-025-00734-4
21. Bozuyuk, U., Wrede, P., Yildiz, E., & Sitti, M. (2024). Roadmap for clinical translation of mobile microrobotics. *Advanced Materials, 36*(23), 2311462. https://doi.org/10.1002/adma.202311462
22. Lee, J. G., Raj, R. R., Day, N. B., & Shields, C. W. (2023). Microrobots for biomedicine: Unsolved challenges and opportunities for translation. *ACS Nano, 17*(15), 14196–14204. https://doi.org/10.1021/acsnano.3c03723
23. Wang, B., Shen, J., Huang, C., Ye, Z., He, J., Wu, X., Guo, Z., Zhang, L., & Xu, T. (2025). Magnetically driven biohybrid blood hydrogel fibres for personalized intracranial tumour therapy under fluoroscopic tracking. *Nature Biomedical Engineering*, *9*, 1471–1485 . https://doi.org/10.1038/s41551-025-01382-z
24. Purcell, E. (1977). Life at low Reynolds number. *American Journal of Physics, 45*(1), 3–11. https://doi.org/10.1119/1.10903
25. Chang, J., Song, Q., Li, R., Xu, R., Dong, C., Li, Z., Liu, L., Lin, T., Bi, Q., & Shen, T. (2024). Design and motion characteristics of a ray-inspired micro-robot made of magnetic film. *Journal of Bionic Engineering, 21*(6), 2745–2758. https://doi.org/10.1007/s42235-024-00588-2
26. Zhao, J., Xin, C., Zhu, J., Xia, N., Hao, B., Liu, X., Tan, Y., Yang, S., Wang, X., Xue, J., Wang, Q., Lu, H., & Zhang, L. (2024).

Insect-scale biped robots based on asymmetrical friction effect induced by magnetic torque. *Advanced Materials, 36*(24), 2312655. https://doi.org/10.1002/adma.202312655
27. Dong, X., Chen, H., Zhou, Z., Ouyang, C., Hu, L., Zhang, F., Chen, B., & Gan, Z. (2024). Salpot: A jet propulsion swimmer with scissor structure and bilateral apertures. *IEEE Robotics and Automation Letters, 9*(8), 7102–7109. https://doi.org/10.1109/LRA.2024.3418278
28. Berg, H. C., & Anderson, R. A. (1973). Bacteria swim by rotating their flagellar filaments. *Nature, 245*(5425), 380–382. https://doi.org/10.1038/245380a0
29. Honda, T., Arai, K., & Ishiyama, K. (1996). Micro swimming mechanisms propelled by external magnetic fields. *IEEE Transactions on Magnetics, 32*(5), 5085–5087. https://doi.org/10.1109/20.539498
30. Bell, D.J., Leutenegger, S., Hammar, K.M., Dong, L.X. & Nelson, B.J. (2007). Flagella-like propulsion for microrobots using a nanocoil and a rotating electromagnetic field. *IEEE International Conference on Robotics and Automation* (1128–1133). Roma. https://doi.org/10.1109/ROBOT.2007.363136
31. Zhang, L., Abbott, J. J., Dong, L., Peyer, K. E., Kratochvil, B. E., Zhang, H., Bergeles, C., & Nelson, B. J. (2009). Characterizing the swimming properties of artificial bacterial flagella. *Nano Letters, 9*(10), 3663–3667. https://doi.org/10.1021/nl901869j
32. Abbott, J. J., Peyer, K. E., Lagomarsino, M. C., Zhang, L., Dong, L., Kaliakatsos, I. K., & Nelson, B. J. (2009). How should microrobots swim? *The International Journal of Robotics Research, 28*(11–12), 1434–1447. https://doi.org/10.1177/0278364909341658
33. Qiu, F., & Nelson, B. J. (2015). Magnetic helical micro-and nanorobots: Toward their biomedical applications. *Engineering, 1*(1), 021–026. https://doi.org/10.15302/J-ENG-2015005
34. Kikuchi, K., Yamazaki, A., Sendoh, M., Ishiyama, K., & Arai, K. I. (2005). Fabrication of a spiral type magnetic micromachine for trailing a wire. *IEEE Transactions on Magnetics, 41*(10), 4012–4014. https://doi.org/10.1109/TMAG.2005.855155
35. Ghosh, A., & Fischer, P. (2009). Controlled propulsion of artificial magnetic nanostructured propellers. *Nano Letters, 9*(6), 2243–2245. https://doi.org/10.1021/nl900186w
36. Yip, W. S., Yan, H. E., Zhang, B., & To, S. (2024). The state-of-art review of ultra-precision machining using text mining: Identification of main themes and recommendations for the future direction. *Wiley Interdisciplinary Reviews: Data Mining and Knowledge Discovery, 14*(1), 1517. https://doi.org/10.1002/widm.1517
37. Zhou, X., Liu, X., & Gu, Z. (2024). Photoresist development for 3d printing of conductive microstructures via two-photon polymerization. *Advanced Materials, 36*(48), 2409326. https://doi.org/10.1002/adma.202409326
38. Yan, H. E., Guo, F., Zhang, B., Chan, Y. K., Zhou, H., Sun, L., He, T., Tang, J., Chen, H., Tan, W., To, S., & Yip, W. S. (2024). Sustainability assessment during machining processes: Evidence from the econ-environmental modelling. *Journal of Cleaner Production, 448*, Article 141612. https://doi.org/10.1016/j.jclepro.2024.141612
39. Guo, F., Yan, E. H., Zhou, H., Xu, Z., To, S., & Yip, W. S. (2024). Technological life-cycle analysis of ultra-precision machining technology: Forecasting perspective directions and tracking the critical transitions with evolution. *Advanced Engineering Informatics, 62*, Article 102805. https://doi.org/10.1016/j.aei.2024.102805
40. Xie, L., Pang, X., Yan, X., Dai, Q., Lin, H., Ye, J., Cheng, Y., Zhao, Q., Ma, X., Zhang, X., Liu, G., & Chen, X. (2020). Photoacoustic imaging-trackable magnetic microswimmers for pathogenic bacterial infection treatment. *ACS Nano, 14*(3), 2880–2893. https://doi.org/10.1021/acsnano.9b06731
41. Dong, S., Yang, T., Lou, Y., Luo, D., Yang, B., Liu, H., Wu, J., & Dong, Y. (2025). A high-precision miniature 3d tactile force sensor based on fiber bragg grating for minimally invasive surgery. *IEEE Transactions on Instrumentation and Measurement, 74*, 1–10. https://doi.org/10.1109/TIM.2025.3571077
42. Dong, S., Liu, Z., Lou, Y., Luo, D., Wu, J., Yang, B., Liu, H., Yang, T., & Dong, Y. (2024). A high-precision miniature triaxial fbg force sensor for detecting tissue anomalies. *Journal of Lightwave Technology, 42*(17), 6143–6152. https://doi.org/10.1109/JLT.2024.3403206
43. Zou, B., Liang, Z., Zhong, D., Cui, Z., Xiao, K., Shao, S., & Ju, J. (2023). Magneto-thermomechanically reprogrammable mechanical metamaterials. *Advanced Materials, 35*(8), 2207349. https://doi.org/10.1002/adma.202207349
44. Chen, C., Ding, S., & Wang, J. (2024). Materials consideration for the design, fabrication and operation of microscale robots. *Nature Reviews Materials, 9*, 159–172. https://doi.org/10.1038/s41578-023-00641-2
45. Tan, L., & Cappelleri, D. J. (2023). Design, fabrication, and characterization of a helical adaptive multi-material microrobot (hammr). *IEEE Robotics and Automation Letters, 8*(3), 1723–1730. https://doi.org/10.1109/LRA.2023.3242164
46. Chen, J., Lei, S., Zhang, S., Zhu, C., Liu, Q., Wang, C., Zhang, Z., Wang, S., Shi, Y., Yin, L., & Wang, R. (2023). Dilute aqueous hybrid electrolyte with regulated core-shell-solvation structure endows safe and low-cost potassium-ion energy storage devices. *Advanced Functional Materials, 33*(19), 2215027. https://doi.org/10.1002/adfm.202215027
47. Zhao, J., Li, X., Tan, Y., Liu, X., Lu, T., & Shi, M. (2022). Smart adhesives via magnetic actuation. *Advanced Materials, 34*(8), 2107748. https://doi.org/10.1002/adma.202107748
48. Zhu, A., Bai, C., Lu, X., Zhu, Y., Wang, K., & Zhu, J. (2024). A magnetic helical miniature robot with soft magnetic-controlled gripper. *IEEE Robotics and Automation Letters, 9*(4), 3163–3170. https://doi.org/10.1109/LRA.2024.3366018
49. Hou, Y., Wang, H., Zhong, S., Qiu, Y., Shi, Q., Sun, T., Huang, Q., & Fukuda, T. (2022). Design and control of a surface-dimple-optimized helical microdrill for motions in high-viscosity fluids. *IEEE/ASME Transactions on Mechatronics, 28*(1), 429–439. https://doi.org/10.1109/TMECH.2022.3201012
50. Tan, L., Yang, Y., Fang, L., & Cappelleri, D. J. (2024). Shape-programmable adaptive multi-material microswimmers for biomedical applications. *Advanced Functional Materials, 34*(34), 2401876. https://doi.org/10.1002/adfm.202401876
51. Jeon, S., Kim, S., Ha, S., Lee, S., Kim, E., Kim, S. Y., Park, S. H., Jeon, J. H., Kim, S. W., Moon, C., Nelson, B. J., Kim, J.-Y., Yu, S.-W., & Choi, H. (2019). Magnetically actuated microrobots as a platform for stem cell transplantation. *Science Robotics, 4*(30), 4317. https://doi.org/10.1126/sciadv.aau9650
52. Zhao, F., Rong, W., Wang, L., & Sun, L. (2023). Photothermal-responsive shape-memory magnetic helical microrobots with programmable addressable shape changes. *ACS Applied Materials & Interfaces, 15*(21), 25942–25951. https://doi.org/10.1021/acsami.3c02986
53. Behrens, M. R., & Ruder, W. C. (2022). Smart magnetic microrobots learn to swim with deep reinforcement learning. *Advanced Intelligent Systems, 4*(10), 2200023. https://doi.org/10.1002/aisy.202200023
54. Amoudruz, L., & Koumoutsakos, P. (2022). Independent control and path planning of microswimmers with a uniform magnetic field. *Advanced Intelligent Systems, 4*(3), 2100183. https://doi.org/10.1002/aisy.202100183
55. Donnelly, C., Hierro-Rodríguez, A., Abert, C., Witte, K., Skoric, L., Sanz-Hernández, D., Finizio, S., Meng, F., McVitie, S., Raabe, J., Suess, D., Cowburn, R., & Fernández-Pacheco, A. (2022). Complex free-space magnetic field textures induced by

three-dimensional magnetic nanostructures. *Nature Nanotechnology, 17*(2), 136–142. https://doi.org/10.1038/s41565-021-01027-7

56. Zeeshan, M. A., Grisch, R., Pellicer, E., Sivaraman, K. M., Peyer, K. E., Sort, J., Özkale, B., Sakar, M. S., Nelson, B. J., & Pané, S. (2014). Hybrid helical magnetic microrobots obtained by 3d template-assisted electrodeposition. *Small, 10*(7), 1284–1288. https://doi.org/10.1002/smll.201302856
57. Li, J., Sattayasamitsathit, S., Dong, R., Gao, W., Tam, R., Feng, X., Ai, S., & Wang, J. (2014). Template electrosynthesis of tailored-made helical nanoswimmers. *Nanoscale, 6*(16), 9415–9420. https://doi.org/10.1039/C3NR04760A
58. Lee, S., Lee, S., Kim, S., Yoon, C.-H., Park, H.-J., Kim, J.-Y., & Choi, H. (2018). Fabrication and characterization of a magnetic drilling actuator for navigation in a three-dimensional phantom vascular network. *Scientific Reports, 8*(1), 3691. https://doi.org/10.1038/s41598-018-22110-5
59. Wang, Z., Fu, D., Xie, D., Fu, S., Wu, J., Wang, S., Wang, F., Ye, Y., Tu, Y., & Peng, F. (2021). Magnetic helical hydrogel motor for directing t cell chemotaxis. *Advanced Functional Materials, 31*(25), 2101648. https://doi.org/10.1002/adfm.202101648
60. Zhao, F., Rong, W., Wang, L., & Sun, L. (2021). Magnetic actuated shape-memory helical microswimmers with programmable recovery behaviors. *Journal of Bionic Engineering, 18*(4), 799–811. https://doi.org/10.1007/s42235-021-0063-6
61. Landers, F. C., Gantenbein, V., Hertle, L., Veciana, A., Llacer-Wintle, J., Chen, X.-Z., Ye, H., Franco, C., Puigmartí-Luis, J., Kim, M., Nelson, B. J., & Pané, S. (2024). On-command disassembly of microrobotic superstructures for transport and delivery of magnetic micromachines. *Advanced Materials, 36*(18), 2310084. https://doi.org/10.1002/adma.202310084
62. Wu, D., Wang, X., Li, R., Wang, C., Ren, Z., Pan, D., Ren, P., Hu, Y., Xin, C., & Zhang, L. (2025). Femtosecond laser-assisted printing of hard magnetic microrobots for swimming upstream in subcentimeter-per-second blood flow. *Science Advances, 11*(27), 1272. https://doi.org/10.1126/sciadv.adw1272
63. Dong, Y., Wang, L., Iacovacci, V., Wang, X., Zhang, L., & Nelson, B. J. (2022). Magnetic helical micro-/nanomachines: recent progress and perspective. *Matter, 5*(1), 77–109. https://doi.org/10.1016/j.matt.2021.10.010
64. Ye, Y., Wu, H., Wu, R., Xu, C., Dong, Y., Zhang, L., & Li, B. (2025). Advanced manufacturing techniques and applications of micro-/nanoscale helices. *International Journal of Extreme Manufacturing, 7*(5), Article 052004. https://doi.org/10.1088/2631-7990/add633
65. Liu, Y., Yang, Y., Yang, X., Yang, L., Shen, Y., & Shang, W. (2021). Multi-functionalized micro-helical capsule robots with superior loading and releasing capabilities. *Journal of Materials Chemistry B, 9*(5), 1441–1451. https://doi.org/10.1039/D0TB02329A
66. Liu, S., Chen, B., Feng, Y., Gao, C., Du, D., Jiang, T., Tu, Y., & Peng, F. (2024). Helical hydrogel micromotors for delivery of neural stem cells and restoration of neural connectivity. *Chemical Engineering Journal, 479*, Article 147745. https://doi.org/10.1016/j.cej.2023.147745
67. Wu, Z., Troll, J., Jeong, H.-H., Wei, Q., Stang, M., Ziemssen, F., Wang, Z., Dong, M., Schnichels, S., Qiu, T., & Fischer, P. (2018). A swarm of slippery micropropellers penetrates the vitreous body of the eye. *Science Advances, 4*(11), 4388. https://doi.org/10.1126/sciadv.aat4388
68. Griffiths, D. J. (2017). *Introduction to Electrodynamics* (4th ed., pp. 255–285). Cambridge University Press.
69. Abbott, J. J., Ergeneman, O., Kummer, M. P., Hirt, A. M., & Nelson, B. J. (2007). Modeling magnetic torque and force for controlled manipulation of soft-magnetic bodies. *IEEE Transactions on Robotics, 23*(6), 1247–1252. https://doi.org/10.1109/TRO.2007.910775
70. Wang, X., Hu, C., Pané, S., & Nelson, B. J. (2021). Dynamic modeling of magnetic helical microrobots. *IEEE Robotics and Automation Letters, 7*(2), 1682–1688. https://doi.org/10.1109/LRA.2020.3049112
71. Wang, X., Hu, C., Schurz, L., De Marco, C., Chen, X., Pané, S., & Nelson, B. J. (2018). Surface-chemistry-mediated control of individual magnetic helical microswimmers in a swarm. *ACS Nano, 12*(6), 6210–6217. https://doi.org/10.1021/acsnano.8b02907
72. Gray, J., & Hancock, G. J. (1955). The propulsion of sea-urchin spermatozoa. *Journal of Experimental Biology, 32*(4), 802–814. https://doi.org/10.1242/jeb.32.4.802
73. Cox, R. G. (1970). The motion of long slender bodies in a viscous fluid part 1. General theory. *Journal of Fluid mechanics, 44*(4), 791–810. https://doi.org/10.1017/S002211207000215X
74. Lighthill, J. (1976). Flagellar hydrodynamics. *SIAM Review, 18*(2), 161–230. https://doi.org/10.1137/1018040
75. Hu, N., Ding, L., Wang, A., Zhou, W., Zhang, C., Zhang, B., & Yin, R. (2024). Comprehensive modeling of corkscrew motion in micro-/nano-robots with general helical structures. *Nature Communications, 15*(1), 7399. https://doi.org/10.1038/s41467-024-51518-z
76. Liao, Z., Hou, X., LinHu, E., Sheng, J., Ge, Z., Jiang, B., Hou, X., Liu, J., Li, Z., Huang, Q., Zhao, X. J., Li, N., Gao, Y. J., Zhang, Y., Zhou, J. Q., Wang, X. Y., Liu, J., Xie, X. P., Yang, C. M., … Li, Z. S. (2016). Accuracy of magnetically controlled capsule endoscopy, compared with conventional gastroscopy, in detection of gastric diseases. *Clinical Gastroenterology and Hepatology, 14*(9), 1266–1273. https://doi.org/10.1016/j.cgh.2016.05.013
77. Yang, L., Zhang, M., Yang, Z., Yang, H. & Zhang, L. (2003). Quadmag: A mobile-coil system with enhanced magnetic actuation efficiency and dexterity. *IEEE international conference on robotics and automation* (pp. 4696–4702). London. https://doi.org/10.1109/ICRA48891.2023.10161290
78. Zhu, A., Shi, Q. & Yang, L. (2025). Pentamag: A parallel moving coil system with enhanced degrees of freedom and workspace. *IEEE international conference on real-time computing and robotics* (pp. 697–702). Toyama. https://doi.org/10.1109/RCAR65431.2025.11139665
79. Kwon, J., Sa, J., Lee, S., & Jang, G. (2024). A voltage minimization control method for magnetic navigation systems to enhance the rotating magnetic field. *IEEE Robotics and Automation Letters, 9*(12), 11561–11568. https://doi.org/10.1109/LRA.2024.3495374
80. Yang, L., Zhang, M., Yang, H., Yang, Z. & Zhang, L. (2021). Hybrid magnetic force and torque actuation of miniature helical robots using mobile coils to accelerate blood clot removal. *IEEE/RSJ International Conference on Intelligent Robots and Systems* (pp. 7476–7482). Prague. https://doi.org/10.1109/IROS51168.2021.9636851
81. Nguyen, K. T., Kim, S.-J., Min, H.-K., Hoang, M. C., Go, G., Kang, B., Kim, J., Choi, E., Hong, A., Park, J.-O., & Kim, C.-S. (2020). Guide-wired helical microrobot for percutaneous revascularization in chronic total occlusion in-vivo validation. *IEEE Transactions on Biomedical Engineering, 68*(8), 2490–2498. https://doi.org/10.1109/tbme.2020.3046513
82. Liu, J., Xu, T., & Wu, X. (2023). Model predictive control of magnetic helical swimmers in two-dimensional plane. *IEEE Transactions on Automation Science and Engineering, 21*(2), 1889–1898. https://doi.org/10.1109/TASE.2023.3250701
83. Khalil, I. S., Adel, A., Mahdy, D., Micheal, M. M., Mansour, M., Hamdi, N., & Misra, S. (2019). Magnetic localization and control of helical robots for clearing superficial blood clots. *APL Bioengineering, 3*(2), Article 026104. https://doi.org/10.1063/1.5090872

84. Leclerc, J., Zhao, H., Bao, D., & Becker, A. T. (2020). In vitro design investigation of a rotating helical magnetic swimmer for combined 3-d navigation and blood clot removal. *IEEE Transactions on Robotics, 36*(3), 975–982. https://doi.org/10.1109/TRO.2020.2988636
85. Xu, S., Liu, J., Yang, C., Wu, X., & Xu, T. (2021). A learning-based stable servo control strategy using broad learning system applied for microrobotic control. *IEEE Transactions on Cybernetics, 52*(12), 13727–13737. https://doi.org/10.1109/TCYB.2021.3121080
86. Liu, Y., Wang, Y., Fang, K., Chen, H., Zeng, G., & Yu, J. (2025). Radar-based control of a helical microswimmer in 3-dimensional space with dynamic obstacles. *Cyborg and Bionic Systems, 6*, 0158. https://doi.org/10.34133/cbsystems.0158
87. Zeng, Y., Chen, G., Lian, H., & Bai, K. (2025). Pose estimation of magnetically driven helical robots with eye-in-hand magnetic sensing. *IEEE Robotics and Automation Letters, 10*(5), 4604–4611. https://doi.org/10.1109/LRA.2025.3553048
88. Yasa, I. C., Ceylan, H., Bozuyuk, U., Wild, A.-M., & Sitti, M. (2020). Elucidating the interaction dynamics between microswimmer body and immune system for medical microrobots. *Science Robotics, 5*(43), 3867. https://doi.org/10.1126/scirobotics.aaz3867
89. Jia, Y., Zhu, Z., Jing, X., Lin, J., & Lu, M. (2023). Fabrication and performance evaluation of magnetically driven double curved conical ribbon micro-helical robot. *Materials & Design, 226*, Article 111651. https://doi.org/10.1016/j.matdes.2023.111651
90. Hou, Y., Bai, K., Zhong, S., Zheng, Z., Shi, Q., Huang, Q., Fukuda, T., Li, F., & Wang, H. (2025). Swimming performance enhancement of the magnetic helical microrobots based on surface microstructure modification. *IEEE Robotics and Automation Letters, 10*(6), 5729–5736. https://doi.org/10.1109/LRA.2025.3557225
91. Wang, G., Wang, S., Shi, F., Liu, X., Wang, D., Abuduwayiti, A., Wang, Z., Liu, M., Wu, Y., & Bi, J. (2024). Enhancing swimming performance of magnetic helical microswimmers by surface microstructure. *Langmuir, 40*(33), 17731–17739. https://doi.org/10.1021/acs.langmuir.4c02107
92. Li, R., Jiang, M., Liu, B., Jiang, S., Chen, C., Liang, M., Qu, L., Wang, C., Zhao, G., Hu, Y., Wu, D., Chu, J., & Li, J. (2024). High-performance magnetic metal microrobot prepared by a two-photon polymerization and sintering method. *Lab on a Chip, 24*(4), 832–842. https://doi.org/10.1039/D3LC01084H
93. Li, R., Tao, Y., Li, J., Jin, D., Xin, C., Ji, S., Wang, C., Zhang, Y., Hu, Y., Wu, D., Zhang, L., & Chu, J. (2024). Rapid fabrication of reconfigurable helical microswimmers with environmentally adaptive locomotion. *Light: Advanced Manufacturing, 4*(4), 380–392. https://doi.org/10.37188/lam.2023.029
94. Liu, L., Chen, B., Liu, K., Gao, J., Ye, Y., Wang, Z., Qin, N., Wilson, D. A., Tu, Y., & Peng, F. (2020). Wireless manipulation of magnetic/piezoelectric micromotors for precise neural stem-like cell stimulation. *Advanced Functional Materials, 30*(11), 1910108. https://doi.org/10.1002/adfm.201910108
95. Li, Z., Che, Y., Chen, M., Hu, J., He, P., Sun, X., Wu, X., Yao, Y., Zheng, H., Liu, G., & Yan, X. (2024). Multifunctional spirulina-hybrid helical microswimmers: Imaging and photothermal efficacy enabled by intracellular gold deposition. *Chemical Engineering Journal, 487*, Article 150584. https://doi.org/10.1016/j.cej.2024.150584
96. Bai, X., Tong, H., Wang, C., Li, Y., Tan, Q., Ye, Z., Pan, L., & Zhao, Y. (2022). Helical carbon nanowires for magnetic-field-controlled swimming. *ACS Applied Nano Materials, 5*(7), 9981–9989. https://doi.org/10.1021/acsanm.2c02325
97. Hou, C., Wang, K., Wang, S., Yu, Z., Wang, X., Qu, Z., Cheng, M., Fan, L., & Dong, L. (2024). Artificial bacteria flagella with micro-structured soft-magnetic teeth. *IEEE Transactions on Robotics, 40*, 4719–4732. https://doi.org/10.1109/TRO.2024.3463482
98. Liu, S., Lu, Q., Liang, Z., Du, D., Chen, B., Feng, Y., Gao, C., Jiang, T., Tu, Y., & Peng, F. (2024). Magnetic-driven hydrogel spiral pva/fe3o4 micromotors for targeted photothermal therapy. *Advanced Therapeutics, 7*(7), 2300334. https://doi.org/10.1002/adtp.202300334
99. Liu, X., Wang, L., Xiang, Y., Liao, F., Li, N., Li, J., Wang, J., Wu, Q., Zhou, C., Yang, Y., Kou, Y., Yang, Y., Tang, H., Zhou, N., Wan, C., Yin, Z., Yang, G.-Z., Tao, G., & Zang, J. (2024). Magnetic soft microfiberbots for robotic embolization. *Science Robotics, 9*(87), 2479. https://doi.org/10.1126/scirobotics.adh2479
100. Ma, Z., Qian, Z., Yin, R., Zhang, H., Zhang, W. & Liu, Y. (2021). Unclogging motions of a spiral microrobot acuated by rotating uniform magnetic field for human vessel occlusive diseases. *International Conference on Electronics Technology* (pp. 887–891). Chengdu. https://doi.org/10.1109/ICET51757.2021.9451005
101. Lee, H., Kim, D.-I., Kwon, S.-H., & Park, S. (2021). Magnetically actuated drug delivery helical microrobot with magnetic nanoparticle retrieval ability. *ACS Applied Materials & Interfaces, 13*(17), 19633–19647. https://doi.org/10.1021/acsami.1c01742
102. Zhang, H., Xu, B., Ouyang, Y., Wang, Y., Zhu, H., Huang, G., Cui, J., & Mei, Y. (2022). Shape memory alloy helical microrobots with transformable capability towards vascular occlusion treatment. *Research, 2022*, 1–13. https://doi.org/10.34133/2022/9842752
103. Peng, Q., Wang, S., Han, J., Huang, C., Yu, H., Li, D., Qiu, M., Cheng, S., Wu, C., Cai, M., Fu, S., Chen, B., Wu, X., Du, S., & Xu, T. (2024). Thermal and magnetic dual-responsive catheter-assisted shape memory microrobots for multistage vascular embolization. *Research, 7*, 0339. https://doi.org/10.34133/research.0339
104. Ceylan, H., Dogan, N. O., Yasa, I. C., Musaoglu, M. N., Kulali, Z. U., & Sitti, M. (2021). 3d printed personalized magnetic micromachines from patient blood-derived biomaterials. *Science Advances, 7*(36), 0273. https://doi.org/10.1126/sciadv.abh0273
105. Su, L., Jin, D., Wang, Y., Wang, Q., Pan, C., Jiang, S., Yang, H., Yang, Z., Wang, X., Xia, N., Chan, K. F., Chiu, P. W. Y., Sung, J.J.-Y., & Zhang, L. (2023). Modularized microrobot with lock-and-detachable modules for targeted cell delivery in bile duct. *Science Advances, 9*(50), 0883. https://doi.org/10.1126/sciadv.adj0883
106. Fan, X., Chen, Q., Li, M., Wu, Z., Tong, D., Xie, H., Yang, Z., Sun, L., & Sitti, M. (2025). Machining swarf formation-inspired fabrication of ferrofluidic helical miniature robots with multimodal locomotion capability. *Science Advances, 11*(27), 4411. https://doi.org/10.1126/sciadv.ads4411
107. Zhou, X., Ma, Z., Wang, K., Zhang, G., Ren, D., Zhang, W., Zhang, B., & Yin, R. (2024). Motion control of magnetic-controlled spiral microrobots for in-vitro plaque removal. *IEEE Robotics and Automation Letters, 9*(6), 5671–5678. https://doi.org/10.1109/LRA.2024.3392492
108. Chaluvadi, B., Stewart, K. M., Sperry, A. J., Fu, H. C., & Abbott, J. J. (2020). Kinematic model of a magnetic-microrobot swarm in a rotating magnetic dipole field. *IEEE Robotics and Automation Letters, 5*(2), 2419–2426. https://doi.org/10.1109/LRA.2020.2972857
109. Pane, S., Zhang, M., Iacovacci, V., Zhang, L., & Menciassi, A. (2022). Contrast-enhanced ultrasound tracking of helical propellers with acoustic phase analysis and comparison with color doppler. *APL Bioengineering, 6*(3), Article 036102. https://doi.org/10.1063/5.0097145

110. Servant, A., Qiu, F., Mazza, M., Kostarelos, K., & Nelson, B. J. (2015). Controlled in vivo swimming of a swarm of bacteria-like microrobotic flagella. *Advanced Materials, 27*(19), 2981–2988. https://doi.org/10.1002/adma.201404444
111. Yang, L., Jiang, J., Ji, F., Li, Y., Yung, K.-L., Ferreira, A., & Zhang, L. (2024). Machine learning for micro-and nanorobots. *Nature Machine Intelligence, 6*, 605–618. https://doi.org/10.1038/s42256-024-00859-x
112. Chen, X., Ren, J., Gu, G., & Zou, J. (2024). Dynamic model based neural implicit embedded tracking control approach for dielectric elastomer actuators with rate-dependent viscoelasticity. *IEEE Robotics and Automation Letters, 9*(10), 9031–9038. https://doi.org/10.1109/LRA.2024.3455771
113. Ju, C.-W., Shen, Y., French, E. J., Yi, J., Bi, H., Tian, A., & Lin, Z. (2024). Accurate electronic and optical properties of organic doublet radicals using machine learned range-separated functionals. *The Journal of Physical Chemistry A, 128*(12), 2457–2471. https://doi.org/10.1021/acs.jpca.3c07437
114. Yang, L., Jiang, J., Gao, X., Wang, Q., Dou, Q., & Zhang, L. (2022). Autonomous environment-adaptive microrobot swarm navigation enabled by deep learning-based real-time distribution planning. *Nature Machine Intelligence, 4*(5), 480–493. https://doi.org/10.1038/s42256-022-00482-8
115. Xu, Y., Ge, J., & Ju, C.-W. (2023). Machine learning in energy chemistry: Introduction, challenges and perspectives. *Energy Advances, 2*(7), 896–921. https://doi.org/10.1039/D3YA00057E
116. Li, Y., Huo, Y., Chu, X., & Yang, L. (2024). Automated magnetic microrobot control: From mathematical modeling to machine learning. *Mathematics, 12*(14), 2180. https://doi.org/10.3390/math12142180
117. Fan, Q., Chen, W., Huang, W., Xie, L., Bi, K., & Zhu, Y. (2022). Combined magnetic field decoupling and disturbance rejection control of microrobots based on extended state observer. *IEEE Robotics and Automation Letters, 7*(2), 4032–4039. https://doi.org/10.1109/LRA.2022.3148785
118. Zhao, F., Rong, W., Wang, L., & Sun, L. (2024). Automatic control of magnetic helical microrobots for on-plane docking. *IEEE Transactions on Automation Science and Engineering, 22*, 2395–2404. https://doi.org/10.1109/TASE.2024.3379226
119. Zhong, S., Hou, Y., Shi, Q., Li, Y., Huang, H.-W., Huang, Q., Fukuda, T., & Wang, H. (2023). Spatial constraint-based navigation and emergency replanning adaptive control for magnetic helical microrobots in dynamic environments. *IEEE Transactions on Automation Science and Engineering, 21*(4), 7180–7189. https://doi.org/10.1109/TASE.2023.3339637
120. Zhao, F., Rong, H., & Wang, L. (2025). Automatic control of magnetic helical microrobots docking with target objects in liquid environments. *Journal of Bionic Engineering, 22*(2), 574–584. https://doi.org/10.1007/s42235-025-00649-0
121. Xu, T., Liu, J., Huang, C., Sun, T., & Wu, X. (2021). Discrete-time optimal control of miniature helical swimmers in horizontal plane. *IEEE Transactions on Automation Science and Engineering, 19*(3), 2267–2277. https://doi.org/10.1109/TASE.2021.3079958
122. Liu, J., Wu, X., Huang, C., Manamanchaiyaporn, L., Shang, W., Yan, X., & Xu, T. (2020). 3-d autonomous manipulation system of helical microswimmers with online compensation update. *IEEE Transactions on Automation Science and Engineering, 18*(3), 1380–1391. https://doi.org/10.1109/TASE.2020.3006131
123. Qi, Z., Cai, M., Hao, B., Cao, Y., Su, L., Liu, X., Chan, K. F., Yang, C., & Zhang, L. (2024). Robust 3-d path following control framework for magnetic helical millirobots subject to fluid flow and input saturation. *IEEE Transactions on Cybernetics, 54*(12), 7629–7641. https://doi.org/10.1109/TCYB.2024.3439708
124. Xu, T., Hwang, G., Andreff, N., & Régnier, S. (2015). Planar path following of 3-d steering scaled-up helical microswimmers. *IEEE Transactions on Robotics, 31*(1), 117–127. https://doi.org/10.1109/TRO.2014.2380591
125. Li, M., Deng, X., Zhao, F., Li, M., Liu, S., & Li, M. (2024). Learning automatic navigation control skills for miniature helical robots from human demonstrations. *Engineering Applications of Artificial Intelligence, 137*, Article 109187. https://doi.org/10.1016/j.engappai.2024.109187
126. Cai, M., Wang, Q., Qi, Z., Jin, D., Wu, X., Xu, T., & Zhang, L. (2022). Deep reinforcement learning framework-based flow rate rejection control of soft magnetic miniature robots. *IEEE Transactions on Cybernetics, 53*(12), 7699–7711. https://doi.org/10.1109/TCYB.2022.3199213
127. Wang, H., Qiu, Y., Hou, Y., Shi, Q., Huang, H.-W., Huang, Q., & Fukuda, T. (2024). Deep reinforcement learning-based collision-free navigation for magnetic helical microrobots in dynamic environments. *IEEE Transactions on Automation Science and Engineering, 22*, 7810–7820. https://doi.org/10.1109/TASE.2024.3470810
128. Wang, H., Zhong, S., Zheng, Z., Shi, Q., Sun, T., Huang, Q., & Fukuda, T. (2024). Data-driven parallel adaptive control for magnetic helical microrobots with derivative structure in uncertain environments. *IEEE Transactions on Systems, Man, and Cybernetics: Systems, 54*(7), 4139–4150. https://doi.org/10.1109/TSMC.2024.3374071
129. Wang, Q., Yang, L., Yu, J., Chiu, P. W. Y., Zheng, Y.-P., & Zhang, L. (2020). Real-time magnetic navigation of a rotating colloidal microswarm under ultrasound guidance. *IEEE Transactions on Biomedical Engineering, 67*(12), 3403–3412. https://doi.org/10.1109/TBME.2020.2987045
130. Yang, L., Yu, J., Yang, S., Wang, B., Nelson, B. J., & Zhang, L. (2021). A survey on swarm microrobotics. *IEEE Transactions on Robotics, 38*(3), 1531–1551. https://doi.org/10.1109/TRO.2021.3111788
131. Liu, Y., Chen, H., Zou, Q., Du, X., Wang, Y., & Yu, J. (2023). Automatic navigation of microswarms for dynamic obstacle avoidance. *IEEE Transactions on Robotics, 39*(4), 2770–2785. https://doi.org/10.1109/TRO.2023.3263773
132. Tottori, S., Zhang, L., Peyer, K. E., & Nelson, B. J. (2013). Assembly, disassembly, and anomalous propulsion of microscopic helices. *Nano Letters, 13*(9), 4263–4268. https://doi.org/10.1021/nl402031t
133. Ye, M., Zhou, Y., Zhao, H., Wang, Z., Nelson, B. J., & Wang, X. (2023). A review of soft microrobots: Material, fabrication, and actuation. *Advanced Intelligent Systems, 5*(11), 2300311. https://doi.org/10.1002/aisy.202300311
134. Wang, Y., Du, X., Zhang, H., Zou, Q., Law, J., & Yu, J. (2023). Amphibious miniature soft jumping robot with on-demand in-flight maneuver. *Advanced Science, 10*(18), 2207493. https://doi.org/10.1002/advs.202207493
135. Lee, S., Kim, J.-Y., Kim, J., Hoshiar, A. K., Park, J., Lee, S., Kim, J., Pané, S., Nelson, B. J., & Choi, H. (2020). A needle-type microrobot for targeted drug delivery by affixing to a microtissue. *Advanced Healthcare Materials, 9*(7), 1901697. https://doi.org/10.1002/adhm.201901697
136. Dong, M., Wang, X., Chen, X.-Z., Mushtaq, F., Deng, S., Zhu, C., Torlakcik, H., Terzopoulou, A., Qin, X.-H., Xiao, X., Puigmartí-Luis, J., Choi, H., Pégo, A. P., Shen, Q.-D., & Pané, S. (2020). 3d-printed soft magnetoelectric microswimmers for delivery and differentiation of neuron-like cells. *Advanced Functional Materials, 30*(17), 1910323. https://doi.org/10.1002/adfm.201910323
137. Xu, H., Medina-Sánchez, M., & Schmidt, O. G. (2020). Magnetic micromotors for multiple motile sperm cells capture, transport, and enzymatic release. *Angewandte Chemie International Edition, 59*(35), 15029–15037. https://doi.org/10.1002/anie.202005657

138. Yang, Z., Yang, L., Zhang, M., Xia, N., & Zhang, L. (2022). Ultrasound-guided wired magnetic microrobot with active steering and ejectable tip. *IEEE Transactions on Industrial Electronics, 70*(1), 614–623. https://doi.org/10.1109/TIE.2022.3153809
139. Zhang, M., Yang, L., Yang, H., Su, L., Xue, J., Wang, Q., Hao, B., Jiang, Y., Chan, K. F., Sung, J. J. Y., Ko, H., Liu, X., Wang, L., Ip, B. Y. M., Leung, T. W. H., & Zhang, L. (2025). A magnetically actuated microcatheter with soft rotatable tip for enhanced endovascular access and treatment efficiency. *Science Advances, 11*(25), 1682. https://doi.org/10.1126/sciadv.adv1682
140. Xin, Z., Zhong, S., Wu, A., Zheng, Z., Shi, Q., Huang, Q., Fukuda, T., & Wang, H. (2025). Dynamic control of multimodal motion for bistable soft millirobots in complex environments. *IEEE Transactions on Robotics, 41*, 2662–2676. https://doi.org/10.1109/TRO.2025.3551541
141. Hou, Y., Zhong, S., Zheng, Z., Du, J., Nie, R., Shi, Q., Huang, Q., & Wang, H. (2025). Magnetic shaftless propeller millirobot with multimodal motion for small-scale fluidic manipulation. *Cyborg and Bionic Systems, 6*, 0235. https://doi.org/10.34133/cbsystems.0235
142. Xu, T., Huang, C., Lai, Z., & Wu, X. (2022). Independent control strategy of multiple magnetic flexible millirobots for position control and path following. *IEEE Transactions on Robotics, 38*(5), 2875–2887. https://doi.org/10.1109/TRO.2022.3157147
143. Xu, T., Hao, Z., Huang, C., Yu, J., Zhang, L., & Wu, X. (2022). Multimodal locomotion control of needle-like microrobots assembled by ferromagnetic nanoparticles. *IEEE/ASME Transactions on Mechatronics, 27*(6), 4327–4338. https://doi.org/10.1109/TMECH.2022.3155806
144. Zhong, S., Guo, S., Sun, T., Huang, H.-W., Shi, Q., Huang, Q., Fukuda, T., & Wang, H. (2025). Paired interactions of magnetic millirobots in confined spaces through data-driven disturbance rejection control under global input. *IEEE/ASME Transactions on Mechatronics*. https://doi.org/10.1109/TMECH.2024.3521085